Draft version November 7, 2012
Preprint typeset using LaTeX style emulateapj v. 5/2/11

arXiv:1211.1019v1 [astro-ph.CO] 5 Nov 2012

UNIFYING STATIC ANALYSIS OF GRAVITATIONAL STRUCTURES WITH A SCALE-DEPENDENT SCALAR FIELD GRAVITY AS ALTERNATIVE TO DARK MATTER

D. F. Mota,
Institute of Theoretical Astrophysics, University of Oslo, 0315 Oslo, Norway – E-mail: D.F.Mota@astro.uio.no

V. Salzano,
Fisika Teorikoaren eta Zientziaren Historia Saila, Zientzia eta Teknologia Fakultatea,
Euskal Herriko Unibertsitatea, 644 Posta Kutxatila, 48080 Bilbao, Spain – E-mail: vincenzo.salzano@ehu.es

S. Capozziello, and
Dipartimento di Scienze Fisiche, Universita' degli Studi di Napoli "Federico II" and INFN, Sezione di Napoli, Complesso Universitario di Monte S. Angelo, Via Cinthia, Edificio N, 80126 Napoli, Italy – E-mail: capozzie@na.infn.it

N.R. Napolitano
INAF - Osservatorio Astronomico di Capodimonte, Salita Moiariello 16, I-80131 - Napoli, Italy – E-mail: napolita@na.astro.it

Draft version November 7, 2012

ABSTRACT

We investigate the gravitational effect of a scalar field within scalar-tensor gravity as an alternative of the dark matter. Motivated by results of chameleon models, $f(R)$ gravity and symmetron models, we study a phenomenological scenario where the scalar field has a mass and a coupling constant to the ordinary matter which scale with the local properties of the considered astrophysical system. We analyze the compatibility of this "alternative gravity" scenario at galaxy and galaxy cluster scales. Main results are: 1) the velocity dispersion of elliptical galaxies can be fit remarkably well by a scalar field, with model significance similar to the one obtained if a classical Navarro-Frenk-White dark halo profile is considered; 2) in particular, the analysis of the stellar dynamics and the gas equilibrium on elliptical galaxies has shown that the scalar field can couple with ordinary matter with different strength (different coupling constants) depending on the clustering state of matter components; 3) spiral galaxies and clusters of galaxies combined together show evident correlations among theory parameters (coupling constants and scalar field interaction length) which suggests the generality of the results at all scales and the way toward an unification of the theory for all gravitating systems; 4) the gravitational effects of the scalar field and its viability as an alternative to the dark matter are confirmed by some preliminary test on strong lensing at galaxy cluster scales.

Subject headings: dark matter – galaxies: elliptical and lenticular – galaxies: clusters: intracluster medium – galaxies: spiral – gravitation

1. INTRODUCTION

Dark matter and dark energy are nowadays widely accepted as the main components of our Universe, although reliable clues about their origin, nature and properties are still missing.

There is a long list of possible dark matter candidates ranging from standard to sterile neutrinos, from axions to super-symmetric candidates, from light to super-heavy scalar fields (see e.g. Bertone et al. 2005; Krauss 2006, and references therein), while dark baryons seem to have a minor contribution.

For what it concerns the nature of dark energy, the largest component in the mass-energy balance of the Universe ($\approx 74\%$), a coherent cosmological model explaining all open issues and the related observed phenomena has still to be found.

These two "dark" ingredients are the pillars of the current cosmological "concordance" model, the ΛCDM, where Λ stands for the cosmological constant (Carroll et al. 1992; Sahni & Starobinski 2000) which is assumed to drive the Universe expansion, and CDM stands for Cold Dark Matter. This model provides a good fit to most of the cosmological data (Sanchez et al. 2006; Seljak et al. 2005; Tegmark et al. 2004) but it is also well known that it is affected by many serious theoretical problems that motivate the search of more general candidates for the acceleration-driver counterpart. Such models range from scalar fields rolling down self-interaction potentials to phantom fields, from phenomenological unified models of dark energy and dark matter to alternative theories of gravity (Capozziello 2002; Koivisto & Mota 2006; Li, Barrow & Mota 2007; Capozziello & Francaviglia 2008; Copeland et al. 2006; Manera & Mota 2006; Mota 2008; Padmanabhan 2003; Peebles & Rathra 2003; Koivisto, Mota & Pitrou 2009; Capozziello & De Laurentis 2011).

Among all these candidates, in Mota et al. (2011, Paper I, hereafter) we have focused on a particular scenario, where a scalar field might be used to unify the cosmological scale acceleration of the Universe with the formation and dynamics of gravitational structures by mimicking dark matter on astrophysical scales.

Scalar fields play an important role in connecting cosmology and particle physics (Binetruy 2006; Linde 2008). In particular, we have shown that theories like the chameleon field theories (Khoury & Weltman 2004; Mota & Shaw 2006; Brax et al. 2004), $f(R)$ gravity (Hu & Sawicki 2007; Starobinsky 2007; Capozziello et al. 2003) and symmetron models (Hinterbichler & Khoury 2010; Olive & Pospelov 2008; Davis et al. 2011), all share the fundamental ingredient of a scalar field which couples to matter via gravitational interaction, being short-ranged in highly dense regions, and long-ranged in low density regions. Such a scalar field would be relatively light on cosmological scales, thus describing cosmological evolution without differentiating much from the ΛCDM model, and, at the same time, it would also be able to satisfy local gravity constraints. Moreover, at different astrophysical scales, the effect of the scalar field would be suppressed or enhanced according to the local astrophysical density.

Starting from these broad properties, we propose a new "parametrization" for a massive scalar field theory where we introduce a field mass (or equivalently an interaction length) and a coupling constant with ordinary matter which may change with scale. Our primary goal is to test whether this parametrization, based on the chameleon or symmetron theories, can account for different observational facts, regardless the underlying physical mechanism producing such a scalar field. Some recent papers (Oyaizu et al. 2008; Brax et al. 2012) analyze symmetron and f(R) gravity theories (of which chameleon models are an extension) in the context of structure formation but they are considered as a background cosmology. Here we propose a scaling mechanism for which they can both explain dark energy (on cosmological scales) and dark matter (on astrophysical scales).

In Paper I we studied the feasibility for the scale-dependent scalar field to work on different gravitational scales by using various cosmological indicators: type Ia supernovae and their Hubble diagram, low surface brightness spiral galaxies and their rotation curves, clusters of galaxies and their mass profiles.

Here we extend our analysis to elliptical galaxies and model the velocity dispersion profiles. As we will show later, this will lead us to new results that have made necessary to re-analyze the gravitational objects studied in Paper I (spiral galaxies and clusters of galaxies) and finally unify all evidences in a more general scheme.

The article is organized as follows: In §2 we give a brief but exhaustive summary of all the main properties of the scalar field theory and describe all the main hypothesis underlying our work. In §3 we accurately describe the used astrophysical data and the way we involved them in our analysis. In §4 we show results concerning elliptical galaxies and in §5 we discussion the implications for a unified picture of all the gravitational structures we have considered. Conclusions are drawn in §7.

2. THE SCALAR-TENSOR FIELD THEORY

The most general action governing the dynamics of a scalar field can be written as (Esposito-Farese & Polarski 2001):

$$
\begin{aligned}
S = & \frac{1}{16\pi G_*}\int \mathrm{d}^4x\sqrt{-g}\left\{F(\phi)\mathcal{R} - Z(\phi)(\partial\phi)^2 - V(\phi)\right\} \\
& - \int d^4x\,\mathcal{L}_m(\psi_m^{(i)}, g^i_{\mu\nu})\ , \qquad (1)
\end{aligned}
$$

where g is the determinant of the metric $g_{\mu\nu}$, $\mathcal{R}$ is the Ricci scalar, $\psi_m^{(i)}$ are the various matter fields, $\mathcal{L}_m$ is the Lagrangian density of ordinary matter, ϕ is the scalar field, $F(\phi)$ and $Z(\phi)$ are some functions of the field which regulate its dynamics, and $V(\phi)$ is the scalar field potential. Depending on the expression of the given functions $F(\phi)$ and $Z(\phi)$ and of the potential $V(\phi)$ one can recover "general" scalar field theories, like the chameleon or the symmetron mechanisms. The main consequence of this action is derivable when considering linear perturbations of matter and their related equation: a wide class of theories leads to a perturbation equation like this (Davis et al. 2011; Brax et al. 2004; Bertschinger & Zukin 2008):

$$
\ddot{\delta}_m + 2H\dot{\delta}'_m = \frac{3}{2}\Omega_m H^2\frac{G_{eff}}{G_N}\delta_m\ , \qquad (2)
$$

where of course the dots means time derivatives, k is the wavenumber length, a is the scale factor, H is the Hubble function, δ_m is the matter density contrast and Ω_m is the matter density parameter. The quantity G_{eff} can be interpreted as an *effective* gravitational constant: in general relativity the gravitational coupling G_N is constant while in many alternative theories of gravity, the strength of gravity varies with time and also with place. A time-varying gravitational coupling is a well known properties of scalar-tensor theories and a generic feature of all modified gravity theories where the Newtonian potential and the spatial curvature potential are different (Bertschinger & Zukin 2008; Acquaviva et al. 2005; Clifton et al. 2005). Within the context of massive scalar field models it has the general expression (Gannouji et al. 2009):

$$
G_{eff}(a;\beta,m;k) = G_N\left(1 + 2\beta^2\frac{\frac{k^2}{a^2m^2}}{1+\frac{k^2}{a^2m^2}}\right)\ . \qquad (3)
$$

where β is the coupling constant of the scalar field with matter and, if the field is at the minimum, the scalar field mass is $m^2 = V_{,\phi\phi}$. In particular the term proportional to m^2 results from the scalar field-mediated force, which is negligible if the physical length scale of the perturbation is much larger than the range of the scalar field-mediated force, namely, if $a/k \gg m^{-1}$. In this case the left hand side of Eq. (2) is well approximated by $3\Omega_m^2 H^2\delta_m/2$ and the matter fluctuations grow as in general relativity.

Taking the inverse Fourier transform of Eq. (3) it is straightforward to obtain the corresponding expression of the gravitational potential for a point mass distribution, $\psi(r)$. Remembering that a potential $\propto \frac{1}{r}$ in real space yields a k^{-2} term in Fourier space, we can recognize in Eq. (3) the point-like gravitational potential per unit mass:

$$
\begin{aligned}
\psi(r) = & -\frac{G}{r}\left(1 + 2\beta^2 e^{-mr}\right) = \\
= & -\frac{G}{r}\left(1 + 2\beta^2 e^{-r/L}\right)\ , \qquad (4)
\end{aligned}
$$

where m is the mass of the scalar field, $L \propto m^{-1}$ is the interaction range of the modified gravitational potential, i.e. the length where the scalar field is effective, and β still being the coupling constant between matter and the scalar field. The gravitational potential given in Eq. (4) has been derived for a point-like source, and it has to be generalize to extended systems in a numerical way. Depending on the particular gravitational system we consider, we will adopt different geometrical hypothesis: for cluster of galaxies and elliptical galaxies we will adopt the spherical symmetry, while spiral galaxies will be assumed as thin disks.

The point-like potential can be split in two terms. The *Newtonian* component is:

$$\psi_N(r) = -\frac{GM}{r} \ , \tag{5}$$

and its extended integral is the well-known expression:

$$\Psi_N(r) = -\frac{GM(< r)}{r} \ , \tag{6}$$

where $M(< r)$ is the mass enclosed in a sphere with radius r. The *correction* term coming from the scalar field is:

$$\psi_C(r) = -\frac{GM}{r}\left(2\beta^2 e^{-\frac{r}{L}}\right) \ , \tag{7}$$

so that to obtain the extended integral we have to calculate the following integral:

$$\Psi_C(r) = \int_0^{\infty} r'^2 dr' \int_0^{\pi} \sin\theta' d\theta' \int_0^{2\pi} d\omega' \psi_C(r') \ , \tag{8}$$

where the angular part is analytically derivable, while the radial integral has to be numerically estimated once the mass density is given. A fundamental difference between the corrected and the Newtonian terms is that in the latter the matter outside the spherical shell of radius r does not contribute to the potential, while in the former the external mass distribution enters into the the potential integral, although the contribution is almost negligible in general.

We also observe that a possible dependence of the coupling constant with scale, i.e. $\beta = \beta(r)$, must be considered when evaluating the integral or the physical observable quantities that we will define in following sections. As we do not know what is the possible analytical behavior of $\beta(r)$, in our approach we will consider this quantity as a constant or weakly depending with the scale, i.e. $\mathrm{d}\beta/\mathrm{d}r \approx 0$, as we will verify *a posteriori*.

2.1. *Hypothesis*

In this section we want to describe in more details what are the main properties and requirements of our parametrization and the motivation of our approach and finally discuss the comparison with observations.

In Paper I we performed our analysis by assuming one single scalar field working for any considered gravitational scale. This scalar field was characterized by a mass (or interaction length L), which should be related to the dimension of the gravitating structure under exam, and by a coupling constant β with the "kind of" *matter* which constitutes the object. We have started by the hypothesis that the *matter* was made only by the observed baryons (hot gas and galaxies in clusters of galaxies; gas and stars in spiral galaxies) with the scalar field generating a dynamical effect similar to the "classical" dark matter. In practice, we replaced the eventual new and exotic dark matter component with an *effective* mass induced by modified gravitational interaction from the scalar field with ordinary matter.

It is important to stress that the coupling constant β was assumed to be *unique* and fixed for all the mass components. As we will discuss in §4, this turns out not be the case for elliptical galaxies, where we will consider the possibility that the scalar field coupling constant shall have different values depending on the different mass components of a galaxy.

This eventuality might have two implications: 1) we have two separate values for the coupling constants each for any baryonic mass component (i.e. stars and gas), or 2) we have only one coupling constant but its measurement might be affected by the matter state.

It is possible to demonstrate that these two options are only apparently conflicting with each other.

Indeed, in the first case the scalar field theory predicts that the field can couple in different ways with different kinds of matter (see e.g., (Brax et al. 2004)). In a classical approach (i.e. general relativity plus dark matter) this would mean that the scalar field can couple differently with *ordinary* matter (baryons, neutrinos, quarks, and so on) and with dark matter.

In the second case, the different measurements depending on the clustered states of the matter can be a consequence of a screening effect which can suppress the field effects and produce an apparent (measured) lower value of the coupling constant β. Such a screening effect is called "thin-shell effect" in the chameleon theory and a similar effect is also present in the symmetron theory. It mainly affects gravitational systems where the inner value of the scalar field is different from the background one and also reflects in a comparison between the inner and the external matter density (Brax et al. 2004; Capozziello & Tsujikawa 2008; Davis et al. 2011).

We *suggest* a possible mixed scenario to make coexistent the two options above.

Let us take the case of a cluster of galaxies and the galaxies and the gas inside it (or star and gas in a galaxy on smaller scale): if the scalar field scales with the density, we can argue that there are two scalar fields, one driving the formation and the dynamics of the cluster and another one driving the formation and the dynamics of the galaxies inside it. We can think that all the substructures inside the cluster experience the cluster-scale scalar field but, as long as the systems evolve, there is a point where the (over–)densities representing the galaxies are as large as the one of the cluster itself and a screening effect arises and wash the cluster-scale scalar field effect out. This process would result in a suppression of the coupling constant of the cluster-scale scalar field with matter in galaxies, such as these latter can be considered as clustered small structures in a larger one.

In this picture, the more diffuse hot gas component mainly present at the cluster scale, can be considered as having only one typical scale, the one of the cluster. This assumption is valid provided that the hydrostatic equilibrium is realized. In this case, the scalar field-gas coupling constant should contain information about the cluster–scale scalar field. The same assumption cannot be made for galaxy systems, as spiral and elliptical galaxies, where the gas can be strongly disturbed by local phenomena (as stellar winds, supernovae, radio jets by active nuclei etc.).

Within this framework, the total potential can be written in two equivalent ways. We can define:

$$\Psi(r) = \Psi_N(r) + \Psi_C(r) \; , \tag{9}$$

if we want to separate the correction that the scalar field provide to the gravitational potential from the classical Newtonian term. Alternatively, we can write:

$$\Psi(r) = \Psi_{star}(r) + \Psi_{gas}(r) \; , \tag{10}$$

where the suffix *star* refers to star component in galaxies, but it can be replaced by *galaxy* when writing the cluster potentials. Each of the two terms is finally given by:

$$\Psi_{star}(r) = \Psi_{N,star}(r) + \Psi_{C,star}(r; \beta_{star}, L) \; , \tag{11}$$

and

$$\Psi_{gas}(r) = \Psi_{N,gas}(r) + \Psi_{C,gas}(r; \beta_{gas}, L) \; ; \tag{12}$$

where we point out that the same scalar field (with mass $\propto L^{-1}$) can interact differently with ordinary matter (two values for the coupling constant, β_{star} and β_{gas}) depending on their clustering state.

Finally, we have to remark here that our approach is implicitly making a *static* assumption for the gravitational structures we consider. This means that, for the moment, we are ignoring that: 1) the values of the scalar field parameters could be subjected to temporal evolution, so that an analysis of how perturbations and overdensity collapse work would be necessary; and 2) a dynamical analysis under the influence of a scalar field should be performed to verify the stability of such gravitational systems.

3. ANALYSIS PROCEDURES

As pointed out in §1, we want to test the scalar field hypothesis on galactic scale by starting with elliptical galaxies.

Differently from spiral galaxies, whose easy interpretable flat rotation curves have been one of the first historical evidences for dark matter, elliptical galaxies are pressure supported systems dominated by hot random motions. The orbital distribution of stars is very difficult to be modeled and consequently also the mass distribution is highly uncertain, because of the well known mass–anisotropy degeneracy.

One way to have some insight on the internal dynamics is to use the information stored in the line–of–sight velocity dispersion as a function of position by inverting the solving the Jeans equations. Under spherical symmetry, and assuming no-rotation, the only effective equation governing the galaxy equilibrium is the radial Jeans equation:

$$\frac{\mathrm{d}(\ell\,\sigma_r^2)}{\mathrm{d}r} + 2\frac{\beta_a}{r}\,\ell\,\sigma_r^2 = -\ell\,\frac{\mathrm{d}\Psi(r)}{\mathrm{d}r} \; , \tag{13}$$

where $\ell(r)$ is the luminosity density of the galaxy, $\sigma_r(r)$ is its radial velocity dispersion. The anisotropy parameter is defined as:

$$\beta_a = 1 - \frac{\sigma_t^2}{\sigma_r^2} \tag{14}$$

where σ_t is the one-dimensional tangential velocity dispersion (defined as a combination of the two angular components of the velocity dispersion tensor $\sigma_t^2 = (\sigma_\theta^2 + \sigma_\varphi^2)/2$ and σ_r the radial component. When $\sigma_t = \sigma_r$, the system is isotropic and $\beta_a = 0$. Instead, when $\beta_a = 1$ the system is fully radial anisotropic while for $\beta_a \to -\infty$ it is fully tangential.

In the Eq. (13), the unknown quantities are the anisotropy parameter and the mass which generates the potential, while $\ell(r)$ is given by the tracer distribution. Thus, different combinations of orbital anisotropy and radial distribution of the mass can produce the same observed dispersion profile. This mass–anisotropy degeneracy can be solved by using independent measurement for the mass. One possibility for that is to use the information from X-ray emission from the hot gas (Mathews & Brighenti 2003), i.e. density and temperature, to solve the hydrostatic balance within the galaxy potential, provided that the gas is at the hydrostatic equilibrium. This is not always true in elliptical galaxies (Diehl & Statler 2007; Humphrey et al. 2006).

Despite all these modeling complications, Jeans analysis has been extensively used in elliptical galaxies, taking great advantage of discrete kinematical tracers probing the gravitational potential out to many effective radii ($R_{\rm eff}$). Globular clusters (Puzia et al. 2004; Bergond et al. 2006; Romanowsky et al. 2009; Shen & Gebhardt 2010; Schuberth 2010; Woodley et al. 2010) or planetary nebulae (PNe, see e.g. Napolitano et al. 2001, 2002; Méndez et al. 2001; Peng et al. 2004; Douglas et al. 2007; Coccato et al. 2009; Teodorescu et al. 2010; Napolitano et al. 2011) have made possible to extend kinematics up to 5-7 $R_{\rm eff}$. Furthermore, the analysis of satellite orbiting around the galaxies could extend up to 50-500 kpc ($\lesssim 10\ R_{\rm eff}$) (Klypin & Prada 2009). However, while globular clusters have classically been used as mass tracers for bright galaxies, being their samples too small in ordinary elliptical galaxies, PNe have been systematically used to map the mass profile of ellipticals (see e.g. Romanowsky et al. 2003; Napolitano et al. 2009, Napolitano et al. 2011, N+11 hereafter, and references there in).

The selection of viable objects for our analysis has been made within the elliptical galaxy sample, observed with the Planetary Nebula Spectrograph (Douglas et al. 2002) and presented in (Coccato et al. 2009, C+09 hereafter), where stellar kinematics of the central regions are combined with PN kinematics of the galaxy regions outside the $R_{\rm eff}$. Adding PNe data has given strong hints about the mass profiles of elliptical galaxies, but has also opened much more questions and nowadays many alternative scenarios are equally feasible. Two exemplary cases are (Romanowsky et al. 2003) and (Dekel et al. 2005): in the former, using the PNe, the galaxies velocity dispersion profiles are found to decline with radius and dynamical modeling of the data indicates the presence of little if any dark matter in these galaxies halos; in the latter, starting from disc-galaxy merger simulations, the lower than expected velocities are in fact compatible with galaxy formation in dark matter halos, thus depending on inner dynamics (elongated orbits) or on projection effects.

For our analysis, we are interested on galaxies that have both extended (stellar) kinematics and published X-rays observations (e.g. Fukazawa et al. 2006). This because we want to explore the dependence of the scalar field dynamics on the mass component of the gravitational systems under exam.

From the 16 galaxies reported in C+09, the only galaxy which had a complete dataset for our purpose is NGC 4374 since other galaxies for which both long slit and PN kinematics were available, like NGC 3377, NGC 3379 and NGC 4494, did not have a reliable deprojected X-ray emitting gas density profile[1]. All the needed photometric properties of NGC 4374 are reported in Table 1.

3.1. *Velocity dispersion analysis*

The general solution to the Jeans equation, Eq. (13), is:

$$\ell(r)\sigma_r^2(r) = \frac{1}{f(r)}\int_r^\infty f(s)\,\ell(s)\frac{\mathrm{d}\Psi(s)}{\mathrm{d}s}\mathrm{d}s \;, \tag{15}$$

where the function f is the solution to

$$\frac{\mathrm{d}\ln f}{\mathrm{d}\ln r} = 2\beta_a(r) \;. \tag{16}$$

By projecting the velocity ellipsoid along the line of sight one can derive the line-of-sight velocity dispersion, which is the kinematical quantity to compare to the observed equivalent ones reported in C+09:

$$\frac{1}{2}I(R)\sigma_{los}^2(R) = \int_R^\infty \frac{\ell\,\sigma_r^2\,r}{\sqrt{r^2-R^2}}\mathrm{d}r + - R^2\int_R^\infty \frac{\beta_a\,\ell\,\sigma_r^2}{r\sqrt{r^2-R^2}}\mathrm{d}r \;, \tag{17}$$

where R is the projected distance from the center of the galaxy and $I(R)$ is the stellar surface brightness profile. To calculate the line-of-sight velocity dispersion one needs two ingredients: an analytical expression for the anisotropy function and the total gravitational potential. For what concerns the anisotropy function, the usual way of proceeding is to compare observations with profiles derived from cosmological N-body simulations. One could use different forms: from the simplest hypothesis of isotropy ($\beta_a = 0$), to a constant anisotropy profile; another commonly used model is the Osipkov-Merritt one, which however provides a poor fit to the simulations. We decided to work with the anisotropy model given in Mamon & Lokas (2005A,B, 2006):

$$\beta_a(r) = \frac{1}{2}\frac{r}{r+r_a} \;, \tag{18}$$

where r_a is a typical anisotropy length, assumed to be $r_a \simeq 14\,R_{eff}$, this value thus providing a good fit to data from dissipation-less cosmological N-body simulations (for a more exhaustive discussion about reliable anisotropy models see Fig. 2 and Section 3.2 of (Mamon & Lokas 2005B).

Then, for calculating the gravitational potential, we need to model the galaxy components, that in this case are: stars, hot gas and the central black hole.

The stellar luminosity density can be obtained by deprojecting the observed surface brightness profile; galaxies in our sample are fitted with the well known and mostly used Sersic profile, i.e.:

$$I(R) = I_0 \exp\left[-\left(\frac{R}{a_s}\right)^{1/m}\right] \;, \tag{19}$$

where I_0 is the central surface brightness (in units of $\mathrm{L}_\odot$ pc^{-2}), a_s the Sersic scale parameter and m the Sersic shape parameter. Starting from this relation, the luminosity density can be obtained by the approximation first proposed in (Prugniel & Simien 1994):

$$\ell(r) \equiv \ell_1\widetilde{\ell}(r/a_s) \;, \tag{20}$$

with:

$$\widetilde{\ell}(x) \simeq x^{-p}\,\exp(-x^{1/m}) \;, \tag{21}$$

$$\ell_1 = \frac{L_{tot}}{4\pi\,m\,\Gamma[(3-p)m]a_s^3} \;, \tag{22}$$

where the function p is defined in (Lima Neto, Gerbal & Marquez 1999) as

$$p \simeq 1.0 - 0.6097/m + 0.05463/m^2 \;, \tag{23}$$

and where the total galaxy luminosity (in solar units) in the V-band where observations for NGC4374 were performed is:

$$L_{tot} = 10^{-0.4(B_T-\mu_D-C_{BV}-M_{B,\odot})} \;, \tag{24}$$

where B_T is the B-band apparent magnitude, $M_\odot$ is the Sun absolute magnitude in the V-band, C_{BV} is the galaxy color, needed to convert all luminosity parameters from the band B to the band V (it is obtained from the extragalactic database *Hyperleda*[2]) and μ_D is the modulus distance (given in Table 1). We also need:

$$I_0 = \frac{L_{tot}}{2\pi\,m\,\Gamma[2m]a_s^2} \;. \tag{25}$$

which appears in Eq. (17) through the surface brightness expression $I(R)$.

The central black hole is assumed to have a constant density inside its typical size, the Schwarzschild radius r_{BH}, which is:

$$r_{BH} = \frac{2\,G_N\,M_{BH}}{c^2} \;, \tag{26}$$

where of course G_N is the Newton gravitational constant and c the light velocity. Then the black hole mass M_{BH} is obtained using the relation which exists between a super massive black hole and the host galaxy luminosity (Gultekin et al. 2009):

$$M_{BH} = 10^{8.95+1.11\cdot\log[10,L_{tot}/10^{11}]} \;. \tag{27}$$

The density is assumed to be null outside r_{BH}.

The gas profiles are assumed to follow the traditionally used β-model[3] (Cavaliere & Fusco-Femiano 1978):

$$\rho_{gas}(r) = \rho_0^{gas}\left(1+\left(\frac{r}{a_g}\right)^2\right)^{3\beta_g/2} \tag{28}$$

---

[1] Fukazawa, private communication.

[2] http://leda.univ-lyon1.fr/

[3] The β_g that appears here does not have any relation with the scalar field coupling constant.

TABLE 1

Elliptical galaxies. Column 1: Galaxy name. Column 2: photometric band. Column 3: modulus distance from Tonry et al. (2001) and shifted by -0.16 mag as explained in Coccato et al. (2009). Column 4: distance of galaxy derived from modulus distance. Columns 5: total B magnitude corrected for extinction and redshift. Columns 6: Sersic scale radius for a $n = 4$ profile (classical De Vaucouleurs profile). Column 7: Sersic scale radius determined from the Sersic fit. Column 8: Sersic shape parameter. Column 9: Stellar Surface brightness at a_s. Column 10: maximum distance from the galaxy center of PNe derived kinematics (maximum distance from the galaxy center of PNe detections).

name	band	μ_D	D	B_T	$a_s^{(4)}$	a_s	m	μ_s	R_{LAST}
			(Mpc)		(kpc)	(kpc)		(mag arcsec^{-2})	(kpc)
NGC4374	V	31.16	17.06	10.01	5.97	9.34	6.11	23.1	25.23 (34.07)

where the central gas density, $\rho_{gas,0}$, the gas core length, a_g, and the constant β_g are derived by fitting mass profiles provided by (Fukazawa et al. 2006).

We remember that in the classical Newtonian approach the total dynamical mass is made of two counterparts, dark matter and baryons (stars, gas and black hole), so that:

$$\begin{aligned} M_{tot}(r) &= \frac{r^2}{G}\frac{\mathrm{d}\Psi_N}{\mathrm{d}r} = \\ &= \frac{r^2}{G}\left(\frac{\mathrm{d}\Psi_{N,bar}}{\mathrm{d}r} + \frac{\mathrm{d}\Psi_{N,DM}}{\mathrm{d}r}\right) = \\ &= M_{bar}(r) + M_{DM}(r) \ , \end{aligned} \tag{29}$$

where of course Ψ_N is the Newtonian potential and:

$$\begin{aligned} \Psi_{N,DM} &\leftrightarrow \rho_{DM} \\ \Psi_{N,bar} &\leftrightarrow \rho_{bar} \sim \rho_{star} + \rho_{gas} + \rho_{BH} \ . \end{aligned} \tag{30}$$

As we pointed out in the § (2), in our approach we have that the total gravitational potential is made of a Newtonian term and a corrective one:

$$\Psi = \Psi_N + \Psi_C \tag{31}$$

so that the dynamical mass is:

$$\begin{aligned} M_{tot}(r) &= \frac{r^2}{G}\frac{\mathrm{d}\Psi_{Ch}}{\mathrm{d}r} = \\ &= \frac{r^2}{G}\left(\frac{\mathrm{d}\Psi_N}{\mathrm{d}r} + \frac{\mathrm{d}\Psi_C}{\mathrm{d}r}\right) = \\ &= M_{bar}(r) + M_{eff}(r) \ , \end{aligned} \tag{32}$$

where the *effective* mass is due to the modification of gravity produced by the scalar field, instead of requiring a new kind of matter as the dark one. Of course, the term Ψ_C has contributions only from visible baryonic mass, i.e. stars, gas and black hole.

By comparing Eq. (29) and Eq. (32) it is straightforward to observe that if we want that the scalar field fits data as well as dark matter we need:

$$M_{eff}(r) \sim M_{DM}(r) \ . \tag{33}$$

For this reason we also realize a fit of our data in the classical context of dark matter in order to perform a comparison between the two approaches. We used the classical Navarro-Frenk-White (NFW) model density given in (Navarro, Frenk & White 1996) by the relation:

$$\rho_{DM}(r) = \rho_0^{DM}\left(\frac{r}{a_d}\right)^{-1}\left[1 + \frac{r}{a_d}\right]^{-2} \ . \tag{34}$$

In (Mamon & Lokas 2005B) more dark matter models are given, one being the generalized NFW model introduced by (Jing & Suto 2000), with inner slope $-3/2$ instead of -1 as it is in the classical NFW profile; and the other one being the convergent model of (Navarro et al. 2004), with an inner slope that is a power-law function of radius. We have verified that using these two models does not give any substantial change in the general mass profiles and in the fitting of velocity dispersion curves, being the classical NFW model sufficient for our requirements. Generally, one is used to convert the quantities appearing in Eq. (34), i.e. (ρ_0^{DM}, a_d) in more useful quantities as the virial radius, r_v, namely the radius enclosing a mass whose mean density is ≈ 100 times the critical density of the Universe, and the concentration parameter, $c_{vir} \equiv \frac{r_v}{a_d}$.

Finally, with all these ingredients, we are able to derive the observed quantity, i.e. the line-of-sight velocity dispersion, σ_{los}. We underline here that the data we consider are derived from the sum in quadrature of two terms: the line-of-sight velocity dispersion and of the rotation velocity. The final quantity, $\sqrt{\sigma_{los}^2 + v^2}$ (see N+11), is a more efficient indicator of the total kinetic energy and is also $\approx \sigma_{los}$ because of the rotation velocity in NGC4374 is not dynamically significant compared to random motion, being ~ 50 km/s^{-1} against a velocity dispersion of $\sim 200 - 250$ km/s^{-1}.

Depending on the approach we consider, σ_{los} will be a function of different parameters: in the classical approach with a NFW density profile for the dark matter component it will be $\sigma_{los} = \sigma_{los}(R; \rho_0^{DM}, a_d, Y_*)$, while in the modified gravity approach by using a scalar field it will be $\sigma_{los} = \sigma_{los}(R; \beta, L, Y_*)$. The quantity Y_* is the stellar mass-to-light ratio we need to convert stellar luminosity density to mass density. For the statistical analysis we will use the chi-square function defined as:

$$\chi^2_{ELL} = \sum_{j=1}^{\mathcal{N}} \frac{(\sigma_{los,th}(R_i; \{\boldsymbol{\theta}_i\}) - \sigma_{los,obs}(R_i))^2}{\sigma_i^2} \tag{35}$$

where $\mathcal{N}$ is the number of data, σ_i^2 the measurement variances and $\{\boldsymbol{\theta}_i\}$ is the parameters theory vector which is, respectively, $\{\boldsymbol{\theta}_i\} = \{\rho_0^{DM}, a_d, Y_*\}$ in the dark matter approach, and $\{\boldsymbol{\theta}_i\} = \{\beta, L, Y_*\}$ in the scalar field approach. For minimizing the χ^2 we use the Markov Chains Monte Carlo Method (MCMC) and test their convergence with the method described by (Dunkley et al. 2005).

4. ELLIPTICAL GALAXIES: RESULTS

In this section we apply the scalar field approach to the elliptical galaxies.

As discussed in §3, the equations of our dynamical approach in the alternative scalar field scenario depend on the parameters that characterize the scalar field properties, i.e. its interaction length L and the coupling constant β (or, as we will discuss, various values for it depending on the number of mass components of each object) and the stellar mass-to-light ratio, Y_*, which we need for the conversion of the stellar surface photometry to the stellar mass density.

Even if the used MCMC method makes it possible to establish some priors on the fitting parameters, we decided to leave them as free as possible; for this reason we have $\beta > 0$ (as in all the expression it enter as β^2, we do not have the possibility to really distinguish between a positive or negative values; moreover, the scalar field theory predicts it to be positive), and $L > 0$ and $Y_* > 0$ as their are positive definite quantities.

To check the validity of our analysis and the ability of deriving information about the scalar field from the observed velocity dispersion as the only kinematical quantity to model, we start by performing an ideal experiment using a mock galaxy with all intrinsic quantities fixed following the same prescriptions of (Mamon & Lokas 2005B).

According to their prescriptions we have considered an elliptical galaxy with a baryon and a dark matter component characterized by the following parameters:

- B-band luminosity $L_{*,B} = 1.88 \times 10^{10}\ h_{70}^{-2}\ L_\odot$ (where $h_{70} = 1$ if $H_0 \equiv 100 \cdot h = 70$ km s^{-1} Mpc^{-1}), from which, using all the relations given in Section 2 of (Mamon & Lokas 2005B), we obtained a Sersic shape parameter $m = 3.12$ and a Sersic length $a_s = 11.6\ h_{70}^{-2}$ pc;
- a typical stellar mass-to-light ratio $Y_* = 6.5$;
- a total mass-to-light ratio $Y = 100$ corresponding to a virial radius, $r_{vir} = 79\ R_{eff}$ and to a concentration parameter $c = 9.70$;
- a black hole to stellar mass ratio $M_{BH}/M_* = 0.0015$;
- a β-model for the gas component with index $\beta_g = -1.5$ and core radius $r_c = R_{eff}/10$.

The velocity dispersion of such mock galaxy is shown in the left panel of Fig. 1 as a dark dashed line. This has a slightly decreasing trend with radius which eventually change its slope outside 50–60 kpc, i.e. well beyond typical radial coverage by PN kinematics.

In fact, we tried to recover (only in a qualitatively way) the total velocity dispersion profile with a scalar field, using Eq. (17) as shown in the left panel of Fig. 1. The scalar field prediction with a single coupling constant ($\beta = 0.05$ and $L \approx 1000$ kpc) (dark dot-dashed line) for all mass components does not match the velocity dispersion profile of the dark matter case (dark dashed line). We can only use such values because the dispersion velocity in the inner region is completely dominated by the stellar component; it works like a sort of "normalization" factor and strongly constrains the value that β can have. A value too much different and higher than this one, would give a completely wrong velocity dispersion reconstruction. In particular, the scalar field total velocity dispersion is almost equivalent to the stellar velocity dispersion (in a classical dark matter scenario) well beyond the radial extent of PNe measurements (vertical dashed line), eventually rising only after this limit.

On the other side, if one assumes a different coupling constant for the two mass components (stars and gas; $\beta_{star} = 0.05$, $\beta_{gas} = 5.6$ and $L \approx 90$) kpc) it is possible to decouple the effects from any of them; in fact, the model which includes two coupling constants (dark solid line) nicely reproduces the velocity dispersion profiles of the classical case, i.e. the scalar field can mimic the profile of a NFW dark halo. We also specify in this context that changing the length parameter r_a which appears in the anisotropy function $\beta_a(r)$ from the chosen best value, $r_a \simeq 14R_{eff}$, to $r_a \simeq 1.4R_{eff}$ (as discussed in (Mamon & Lokas 2005B)), beyond of spanning a wide range of values, does not change our results.

The circular velocity curve, calculated from the relation $v_c^2 = r\ d\Psi/dr$, is instead rather flat out to 100 kpc, clearly showing how dominant is the dark matter in the total galaxy potential. This latter property is what we expect to reproduce with the scalar field. We finally stress that if we had adopted the circular velocity as an observational quantity (as it is done in spiral galaxies), we would not have any chance of discriminating between the two approaches, i.e., one or two coupling constants for the scalar field and the baryonic matter. This is shown in the right panel of Fig. 1 where we can see how the two different cases for the scalar field give two equivalent reproductions of the NFW profile at least in the depicted distance range (the two representing lines, the solid and the dot-dashed one, are indistinguishable as perfectly overlapping); this is an important issue to be considered for when evaluating results for spiral galaxies in next sections.

Starting from this preliminary considerations, we can move to the analysis of a real system: NGC 4374 (see Table 1).

4.1. *NGC4374*

We will make use of the PN sample discussed in N+11 which we refer the reader to for the details of the PN sample properties and the derivation of the kinematical profiles we will use in our analysis; the PN dispersion profile extends out to $\approx 5\mathrm{R}_{eff}$ which is a distance large enough to explore any deviation of the galaxy dynamics from a pure Newtonian no dark matter behavior. N+11 has provided a full Jeans analysis of the system in the ΛCDM framework and showed that the dark matter distribution in this galaxy is nicely consistent with a "standard" NFW halo. In this work, the authors use dispersion–kurtosis constraints in order to alleviate the mass-anisotropy degeneracy.

This galaxy has been also analyzed in the context of $f(R)$ theories (Napolitano et al. 2012), where a Yukawa-like modification of the gravitational potential is adopted as alternative to dark matter. This approach is different from the one we are adopting in the context of the scalar field where the potential allows us to break the contribution of all mass components (stars and gas) which is a peculiar feature of our theoretical scenario that cannot

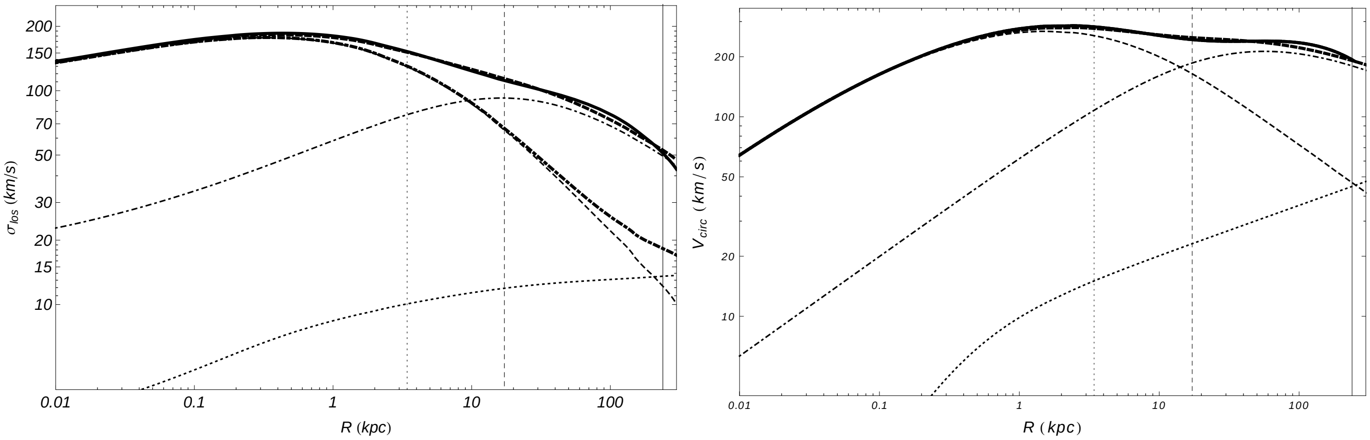

FIG. 1.— Mock elliptical galaxy analysis. *Left panel*: velocity dispersion profile; *Right panel*: circular velocity profile. Dark lines: solid - scalar field with two coupling constants; dot-dashed - scalar field with one coupling constant; dashed - classical NFW dark matter profile. Light lines: dashed - stellar velocity dispersion (circular velocity) in the classical dark matter approach; dotted - gas velocity dispersion (circular velocity) in the classical dark matter approach; dot-dashed - dark matter velocity dispersion (circular velocity). Vertical lines: dotted - effective radius R$_{eff}$, limit achievable with only stellar photometry; dashed - $5-6$ R$_{eff}$, limit achievable with PNe reconstructed kinematics; solid: virial radius r_{vir}.

be included in their physical model.

Before we proceed with the scalar field models as in §3, we have to underline a preliminary but important dynamical choice: the stellar component is the one that dominates the velocity dispersion profile, because it dominates the profile in the inner region and this implies a stronger weight on the global fit to the velocity dispersion. For NGC 4374 there are different literature models of its stellar photometry (mainly depending on the extension of the adopted datasets): a typical De Vaucouleurs profile (a Sersic profile with index $m=4$), with $R_{eff}=5.97$ kpc (Cappellari et al. 2006); a Sersic profile with $R_{eff}=11.69$ kpc and $m=7.98$ (Kormendy et al. 2009); and a Sersic profile with $R_{eff}=9.34$ kpc and $m=6.11$ (N+11). The first model has some problem in fitting data at low distances from the center and can also affect large radii data, as the De Vaucouleurs profile is not always able to describe all the intrinsic features of an elliptical galaxy. The second model allows a better fit to the stellar profile but fails to recover the behavior of surface brightness at small radii ($R \lessapprox 0.5$ kpc). Finally, the third model gives a very good fit of the stellar profile and in a wider range than the previous one, namely, $0.09 \lessapprox R \lessapprox 38$ kpc, out to the distances covered by PNe observations. For this reason we decided to adopt the model profile from N+11 in the following dynamical analysis. Here we adopted two different approaches in order to optimize at the best the goodness of the surface brightness reconstruction: a first one considering all the data, and a second one considering only data points with $R>0.09$ kpc.

We have started by using our model machinery assuming the standard Newton dynamics and a NFW dark halo and cross-check our results with the ones presented in N+11. The results are in Table 2 which somehow differ with the results discussed in their § 3.5.1. Before we go into the details of the discrepancy, we need to remark that there are some critical differences between the two approaches. Here we use some parametrized stellar surface density, while in N+11 they use an interpolated function. Furthermore, we are assuming here an anisotropy profile which is rather different from the one constrained by N+11 where they have used the kurtosis information. These two main differences can produce some substantial divergences in the modeling of the very central data points thus affecting the parameters which are more sensitive to the small radii fit.

For this reason we have repeated the models including all the kinematics data point, and excluding the data at $R>0.09$ kpc and $R>1$ kpc and find substantial differences as shown in Table 2).

In particular, including the whole sample we have obtained a lower value of the central density ρ_0^{DM} and an higher value for the NFW radius a_d with no statistically significant difference between the total and the cut sample, but if we consider the expected relation between these two parameters derivable from a collisionless ΛCDM universe with WMAP5 parameters (Eq. (13) and blue contours of Fig. 7 in N+11), we have correspondence at 1σ level. The concentration parameter, $c \approx 4$, matches with the lower limit of most of the cases shown in the Table 2 of N+11, and in particular with their assumed best reference model (i.e., an adiabatically contracted NFW profile with an anisotropy distribution different from the one adopted here, which should result in a more concentrated dark matter density profile). The virial radius is notably larger; while the virial mass is perfectly consistent with their results even if showing a wider confidence level extending preferentially to higher values. If we compare these results with the Fig. 11 in N+11, we see that our results for the parameters $(c_{vir}, \log M_{vir})$ fall in the region limited by the results inferred from late-type galaxies dynamics and from weak lensing of all type of galaxies and groups (Napolitano et al. 2009); in particular the values coming from the $r>0.09$ kpc sub-sample perfectly match with this last curve. For what it concerns the luminous matter parameter, we found values slightly higher for the stellar mass-to-light ratio, $Y_* \approx 6.6$, that is however perfectly compatible with a Salpeter Initial mass function (Fig. 5 in N+11).

Looking to the left panel of Fig. 2 we see how the stellar component dominates the velocity dispersion profile only

TABLE 2

Elliptical galaxies: NFW dark matter. Column 1: χ^2 type. Column 2: central NFW density. Column 3: NFW radius. Columns 4: stellar mass-to-light ratio in the observation photometric band. Column 5: NFW concentration parameter. Columns 6: virial radius. Column 7: virial mass. Column 8: stellar mass-to-light ratio in the B band.

	$\chi^2/d.o.f.$	ρ_0^{DM} ($10^6\ M_\odot/\mathrm{kpc}^3$)	a_d (kpc)	Y_* ($Y_\odot$)	c_{vir}	$\log M_{vir}$ ($M_\odot$)	r_{vir} (kpc)
χ^2_{all}	39.68/37	$0.361^{+0.296}_{-0.240}$	$316.37^{+693.01}_{-116.73}$	$6.67^{+0.051}_{-0.056}$	$4.01^{+1.22}_{-1.61}$	$13.34^{+2.58}_{-0.54}$	$1269.65^{+4016.29}_{-790.49}$
$\chi^2_{>0.09}$	29.63/33	$0.402^{+0.393}_{-0.203}$	$290.00^{+299.24}_{-119.81}$	$6.66^{+0.060}_{-0.062}$	$4.21^{+1.48}_{-1.16}$	$14.02^{+1.31}_{-1.12}$	$1221.66^{+2130.79}_{-702.81}$
$\chi^2_{>1}$	9.65/17	$0.841^{+1.552}_{-0.506}$	$179.61^{+200.67}_{-93.74}$	$6.28^{+0.263}_{-0.282}$	$5.83^{+3.23}_{-1.95}$	$13.81^{+1.55}_{-1.49}$	$1047.03^{+2397.70}_{-713.89}$

TABLE 3

Elliptical galaxies: Scalar field. Column 1: χ^2 type. Column 2: Coupling constant of scalar field and star component. Column 3: Coupling constant of scalar field and gas component. Column 4: Coupling constant of scalar field and black hole component. Columns 5: Scalar field interaction length. Column 6: stellar mass-to-light ratio in the related band.

	$\chi^2/d.o.f.$	β_{star}	β_{gas}	β_{BH}	L (kpc)	Y_{star} ($Y_\odot$)
χ^2_{all}	38.16/34	$0.100^{+0.229}_{-0.069}$	$10.002^{+0.465}_{-0.528}$	$0.644^{+0.079}_{-0.090}$	$658.26^{+1328.51}_{-410.70}$	$6.099^{+0.166}_{-0.992}$
$\chi^2_{>0.09}$	19.16/31	$0.086^{+0.154}_{-0.065}$	$11.089^{+0.648}_{-0.561}$	$1.167^{+0.116}_{-0.125}$	$183.18^{+2127.44}_{-96.40}$	$5.633^{+0.220}_{-0.499}$

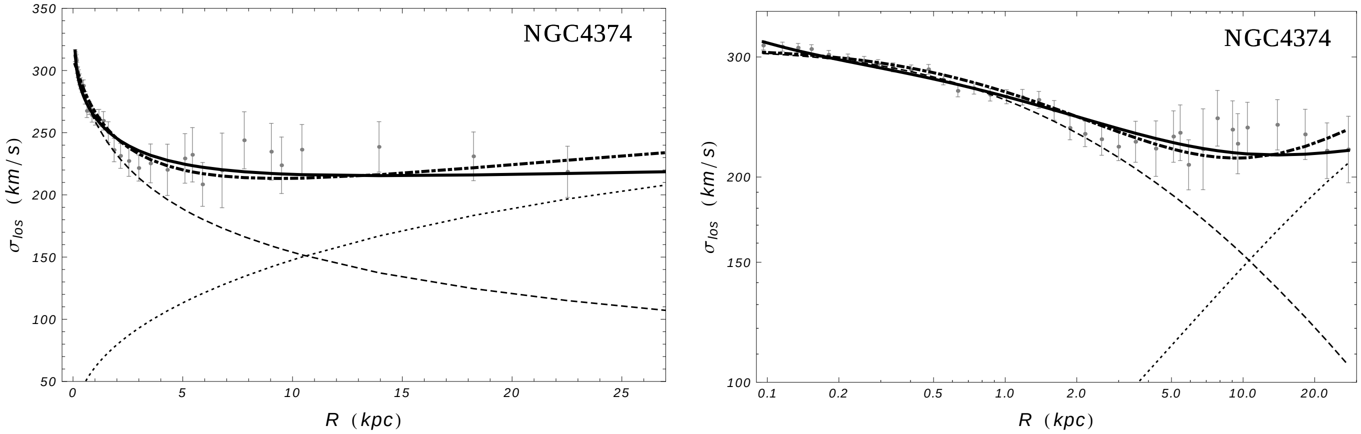

Fig. 2.— *Left panel.* Velocity dispersion curve of NGC4374. Dark lines: solid line is the total velocity dispersion in the scalar field approach, i.e. scalar field + baryons; dot-dashed line is the total velocity dispersion in the classical approach, i.e. dark matter + baryons. Light lines: dashed line is the stellar velocity dispersion in the NFW approach; dotted line is the dark matter velocity dispersion. *Right panel.* The same as before but in logarithmic scale.

in the very central regions ($r \lesssim 1.0$ kpc), with the black hole contribution being important only for very small scales, while the NFW dark matter becomes dominant in the line-of-sight velocity dispersion profile at ≈ 10 kpc which corresponds to $\approx 1-2$ R_{eff}.

Based on this, when using only data with $r > 1.0$ kpc we have been able to recover results more similar to N+11 for what concerns the NFW profile: an higher central density parameter for the dark matter profile (even if it is again lower than the one measured in N+11); a smaller value for the NFW length (but still higher than N+11); the couple $(c_{vir}, \log M_{vir})$ is now compatible both with weak lensing inferred trend and with the relation derived from WMAP5-based simulations; finally, the virial radius is now only a 30% higher than their value.

If we now move to the scalar field alternative approach, it is clear (right panel of Fig. 2) that this is as successful as the classical dark matter approach in modeling the dispersion profile. The largest differences with respect the NFW profile are found both at the very small radii, where the scalar field model shows a steeper slope while the NFW one seems to reach a plateau, and at the very outer region, where the scalar field model stays flatter than the NFW profile, although more extended data would allow to adjust the two model better at the largest distance and possibly recover a better agreement also at shorter scales. However, as seen by the χ^2 results in Table 3, the best fit is also in this case very good and while the NFW and the scalar field approaches are almost equivalent when using all the data points, if we considering the value of the reduced χ^2 (with the NFW χ^2 being slightly smaller than the scalar field one) for the best–fit to the data points with $R > 0.09$, the scalar field turns out to provide a far better significance of the fit with respect the NFW model.

In this case, the stellar mass-to-light ratio is smaller than the NFW-based one and it is now more compatible with the Kroupa IMF (Kroupa 2001) values found in

N+11. Even more importantly, the scalar field parameters turned out to be consistent with what we argued for the double coupling constant hypothesis.

First, the stellar mass component shows the lowest coupling constant among all the mass components, even lower than the black hole one. As anticipated, this can be the consequence of the "average" effect of the screening action made by the scalar field on the stellar component. The same does not happen to the black hole, since this represents a singularity and it is difficult to detail the change in the field from inside to outside and the comparison with its *classical* Newtonian force.

Second, the coupling constant which refers to the gas seems to be mostly correlated with the galaxy gravitational potential and the scalar field mass.

To conclude, we stress that both the classical dark matter approach and the scalar field seem to be unable to describe the small "shoulder" in the dispersion profile that is present at $R \approx 10$kpc, precisely where the PNe data overlap the only stellar kinematics. One may think that this can be a consequence of some unaccounted orbital anisotropy. In fact, this mainly depends on the choice we made to use a parametric form of the star density $\ell(r)$ instead of a smoothed light profile like in N+11 where it was possible to recover all the details of the dispersion profile (with a small degree of radial anisotropy). This means that the observed kinematics is somehow strongly sensitive to the tracer space density distribution.

5. UNIFIED PICTURE

The result obtained with the elliptical galaxy NGC 4374 is not meant to have the sufficient generality to drive any conclusion on the new proposed multi–coupling constant scenario. However, it is not surprising that the proper handling of physically more complex, multicomponent systems like ellipticals has opened new perspectives also in the scalar field approach. If our scenario is correct, this shall be in fact made more evident on gravitational systems where the evolutionary status is different (it is the case of spiral galaxies, as we will show in next sections) or where matter shows very different phases. But a more detailed analysis in this sense is out of the purpose of our work and will be developed in forthcoming papers.

Since we do not expect to extend the elliptical sample any soon, due to the difficulty in finding galaxies having both extended stellar (PNe) kinematics and not faint gas profiles, in this section we try to re-interpret the results of Paper I in terms of the new evidences found for NGC 4374, i.e. the possibility of disentangling the various mass components with respect of the coupling constant with the scalar field. In this respect we aims at drawing a common scenario for all the gravitating systems (galaxies: spirals and ellipticals, and clusters) in a consistent way.

5.1. *Clusters of Galaxies*

By comparing Figs. 3 - 4 with the corresponding figures in Paper I (Figs. 3 - 4 in that paper), we see that the the new approach of using the two mass component has allowed us to improve the model fit in 9 cases, especially at small radii. In one case (RXJ1159) the new approach has produced a remarkable fit where the model in Paper I failed completely. Only for 3 clusters the mass profile reconstruction has not got any benefit by the two component approach, although for all sample the deviation of the best fit from the data in never worse than at 1σ confidence level.

Looking at Table 4 we can quantify better the differences with Paper I: the interaction length slightly diminishes in the most of the objects, still staying compatible with typical cluster scales (≈ 1 Mpc; see also Eq. (36)), while the coupling constant with gas is generally larger than previous estimates. Two objects in particular have very large coupling constant values, i.e. clusters A262 and MKW4.

On the other side, the coupling constant related to galaxies is always much lower than the one of the gas one (as it is expected from the discussion in § 2.1, except for two cases, i.e. clusters A133 and RXJ1159. It is interesting to note that among all these exceptions, two of them (MKW4 and RXJ1159) are considered more similar to group than to real clusters of galaxies or even as extended elliptical galaxies (Vikhlinin et al. 2005), thus for all these systems the argument adopted for normal galaxies might not apply straightforwardly.

For the other two objects no particular features where found in literature to explain the anomalies. We can only remark that A262 seems to be as small as MKW4 (i.e. they share the same data extension) and differently from this latter is believed to be a normal cluster of galaxies in literature. A possible relation between the cluster scale and the gas coupling constant is possible: if we think about this last one as a concentration parameter, we can expect that smaller structures exhibit an higher value for it. For A133 nothing peculiar was found in literature so to justify the high value for the galaxy coupling constant we found; we can only verify that the fit with data is really good. As we did in Paper I we want to find some relations among the scalar field parameters and the physical properties of the considered gravitational systems to establish if this alternative scenario can be a valid alternative to general relativity and dark matter. First of all, in the right panel of Fig. 5 we have a relation between the interaction length, L, and the radius r_{500}, the distance from the center corresponding to an overdensity ≈ 500 times relative to the critical density at the cluster redshift. We prefer this quantity with respect of the virial radius r_{vir} used in Paper I because while the latter is derived using a relation coming from cosmological simulations (Bryan & Norman 1998; Evrard et al. 1996) and thus depending on the gas-weighted average temperature of the cluster, the former is derived in (Vikhlinin et al. 2005) directly from observational data by using the hydrostatic equilibrium equation. We have also verified that the two distances are proportional, having $r_{500} \propto r_{vir}^{1.039}$.

The relation between the scalar field length L and the radius r_{500} is derived from an error weighted fit excluding the previously described four peculiar clusters (right panel of Fig. 5):

$$\log L = (-1.59 \pm 0.82) + (1.49 \pm 0.27) \cdot \log r_{500} \ . \quad (36)$$

We have also found a relation between L and the average gas-weighted temperature $< T >$, left panel of Fig. 5:

$$\log L = (2.45 \pm 0.11) + (0.68 \pm 0.17) \cdot \log < T > \ . \quad (37)$$

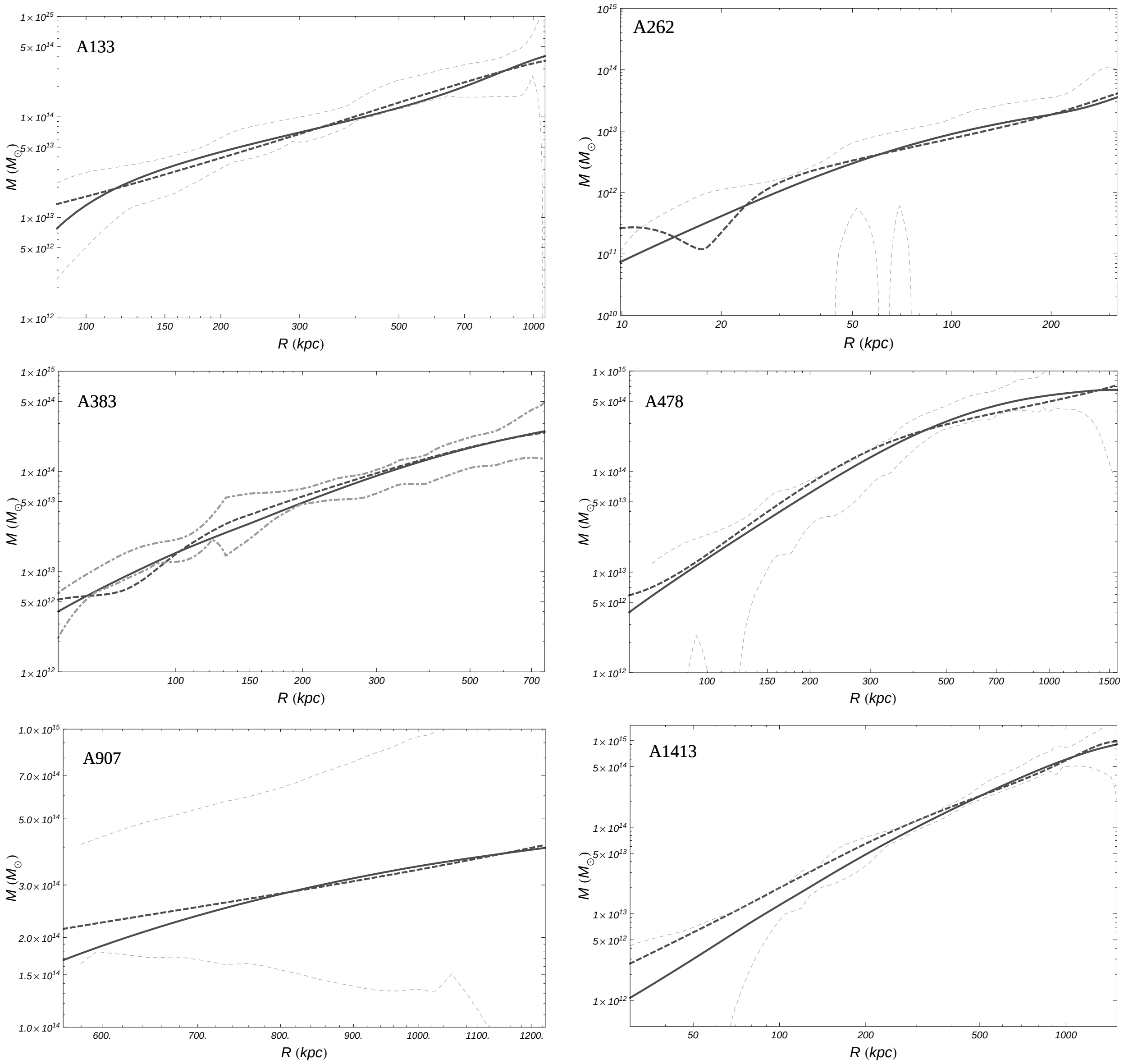

FIG. 3.— Dark matter profile vs radii for clusters of galaxies. Dashed line is the observationally derived estimation of dark matter; solid line is the theoretical estimation for the effective dark matter component; dot-dashed lines are the 1-σ confidence levels given by errors on fitting parameters plus statistical errors on mass profiles.

As we pointed out in Paper I, there exists a relation between the cluster mass and average temperature, i.e.:

$$M_\Delta/T^{3/2} \propto H_0/H(z)\ , \tag{38}$$

where Δ is the overdensity level relative to the critical density at the cluster redshift, so that $M_{180} = M_{vir}$. With the previous phenomenological expressions holding, this mass-temperature relation can be easily converted in:

$$L^{0.27} \propto H(z)/H_0\,. \tag{39}$$

In Fig. 6 we can verify that assuming a fiducial WMAP quintessence model[4], with $\Omega_m = 0.259$ and $w = -1.12$, and assuming $H_0 = 72.4$ km s^{-1} Mpc^{-1}, the previous relation is able to match the chosen fiducial model following the relation $H(z)/H_0 = (0.169 \pm 0.006)L^{0.27}$.

In Figs. 7 we also represent the scaled temperature profiles versus the distance from the center of any cluster scaled with respect to the scalar field length obtained by fit, showing the same good reproduction of the self-similarity that characterizes the classical dark matter approach and, as we found in Paper I, the absence of the subgroups which clusters are divided in depending on the mean temperature values (Vikhlinin et al. 2005). The only exception with respect of Paper I is A133, which now appears to be to more stretched down, even if no peculiar elements have been found in literature and no problems in performing its analysis have been encountered.

5.2. *LSB spiral galaxies*

---

[4] http://lambda.gsfc.nasa.gov/product/map/current/parameters.cfm

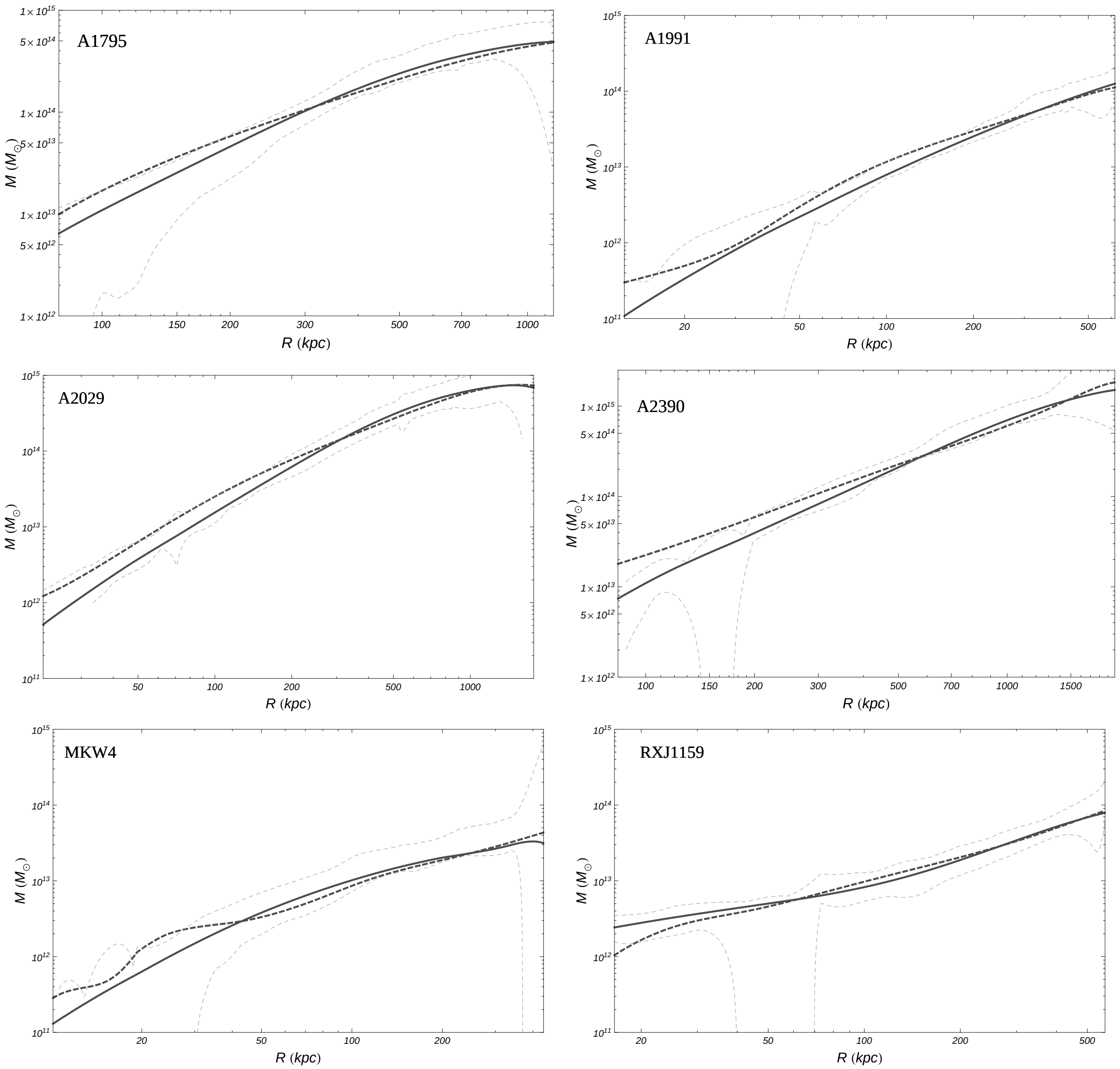

FIG. 4.— Same of Fig. (3).

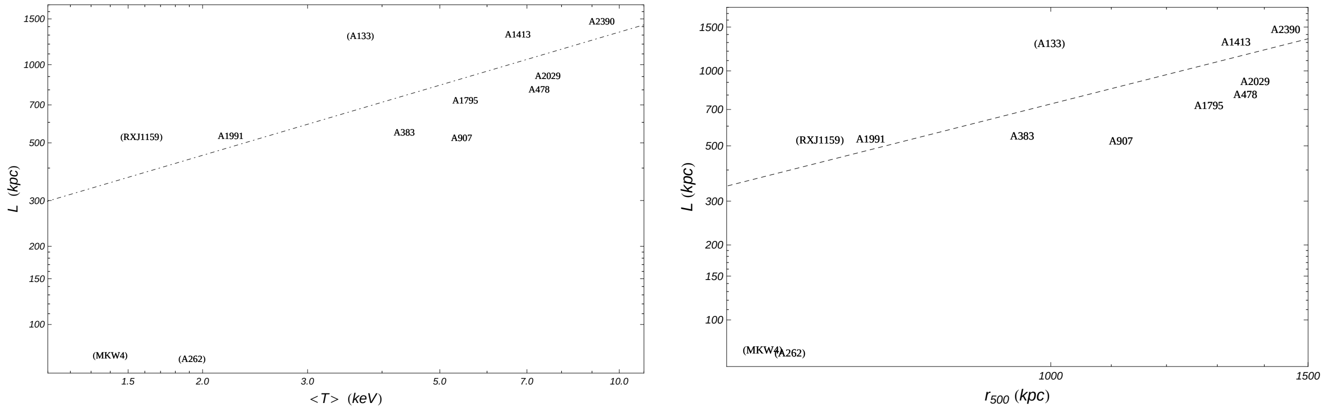

FIG. 5.— Scalar field length plotted versus mean (gas-density weighted) cluster temperature and the radius r_{500} defined in the text.

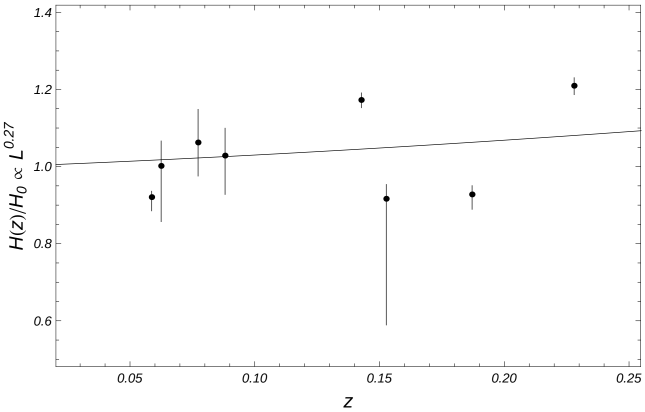

FIG. 6.— Comparison between the Hubble function $H(z)$ calculated from the fiducial model described in the text and the Hubble function obtained by the empirical relation $H(z) \propto L^{0.27}$. Error bars are calculated from the errors on the interaction length L.

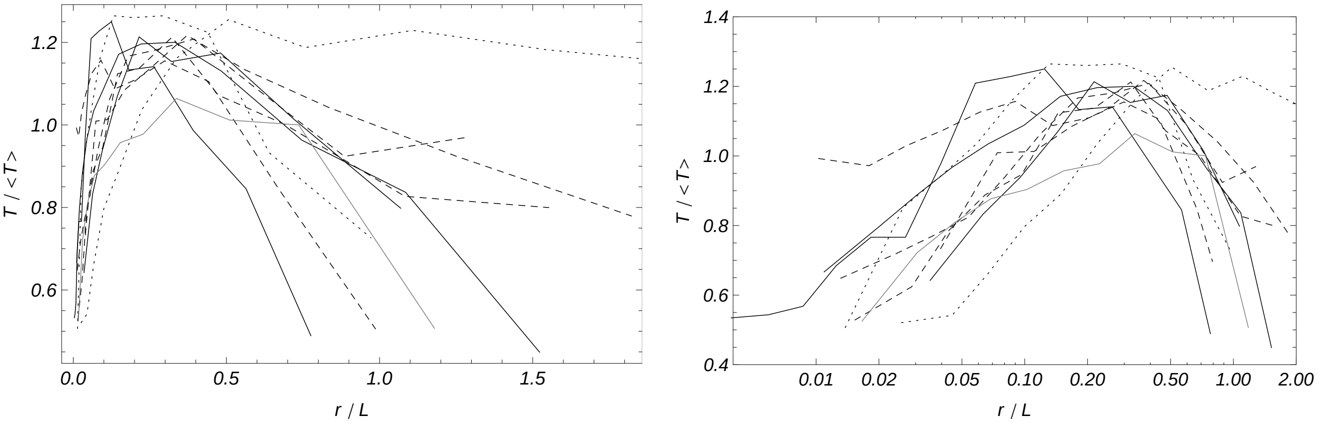

FIG. 7.— Temperature profiles for all clusters plotted as a function of distance from the center and in units of the scalar field length L. The temperatures are scaled to the mean (gas-density weighted) cluster temperature. Dashed line is for high temperature clusters ($< T > > 5$ keV); solid line is for intermediate temperature clusters ($2.5 < < T > < 5$ keV); dotted line is for low temperature clusters ($< T > < 2.5$ keV).

We now consider the case of spiral galaxies. The modeling of these systems involves the same number of parameters of elliptical galaxies, i.e. the parameters associated to the scalar field and the stellar mass-to-light ratio, Y_*. As discussed for the elliptical case, the latter parameter cannot vary arbitrarily but has to be consistent with stellar population models. As for spiral systems one can expect Y_* to vary in the range ≈ 0.5 and ≈ 2 for the galaxy sample that we have adopted in this work, we have decided to be conservative and leave the model parameters to vary in the interval $[0; 5]$ (for any further and detailed description see Paper I).

Before we proceed to illustrate the results, we need to remark that the two component approach, for the spiral galaxies, can suffer of some additional noise source with respect the analysis performed on paper I and can somehow affect the results. As we have exhaustively discussed in Paper I, the gas data are very noisy and in some cases they can also show particular features which are unavoidable due to intrinsic dynamical properties (e.g. negative velocities due to counter rotating discs, large scatter from non-circular motion, etc.). While these effects have been mitigated in Paper I, where using stars and gas together allowed the more circular velocity of stars to dilute the noisy features of the gas, here the gas component to the scalar field might result highly uncertain and cause an higher value for the gas coupling constant than the one of stars. In order to improve the accuracy of the fit for the gas component, we have tried in this work to obtain a more accurate fit of the gas density: the result of this new analysis is evident in the smoother trend of most of the galaxies.

The new models of the spiral rotation curves seems to give results that are less clear than the one obtained for clusters in the previous section (see Figs. 8 - 9): by decoupling the gas and the star components, we do not gain much in the quality of the fits (except a slightly better accordance to data of NGC4173 and NGC9211, where the models are closer to the ones obtained in Paper I). This is the consequence of the evidence showed in the previous section when testing the method on elliptical galaxies. We have seen that the effect of the decoupling of the mass components does not show up in the circular velocity but only the velocity dispersion. In the LSB analysis, as we are modeling the circular velocity we should expect a minimal improvement by the addition of a further coupling constant which implies that we are limited to reliably decouple the different mass components in spiral galaxies because of the unsuitability of the dynamical probe (the rotation curve).

Of course, we remind that this *inducted* idea has to be considered with caution, since elliptical and spiral galaxies are completely different gravitational structures from a dynamical point of view: elliptical galaxies are dominated by random motions while spiral galaxies are dominated by ordered (rotational) motions. Moreover we can add another element which make our global results more homogeneous and consistent each other: the decoupling (with an effective improvement in fits) is given for elliptical galaxies and clusters of galaxies, which are both hot systems (i.e. dominated by random motions) and are supposed to be virialized, while this does not happen for spiral galaxies. Thus it is possible that the possibility of decoupling the different mass components is related to the reached equilibrium in those two kinds of gravitational structures, while in spiral galaxies stars and gas are again more strictly correlated. In that case, we would have also a correlation of our scalar field analysis with the evolutionary state of the gravitational objects; but to verify this is out of the purpose of this paper.

For all these reasons we have proceeded with the star and gas component decoupling approach also for LSB systems and we have found we have a clear distinct behavior for the coupling constants. First of all, unsurprisingly the gas coupling constant seems to be very similar to the only one coupling constant of Paper I, and it is very well constrained in the range $[1.1; 2.1]$ with only 4 exception: UGC3851, which has the smallest value (as in Paper I); UGC4173, which has a smaller than unity value, but still being compatible with the previous range at the highest 1σ confidence limit; UGC4325 and UGC5721 which have larger values. This means that the dominant coupling constant for LSBs is the one from the gas.

On the other side, the stellar coupling constant shows a two-fold behavior: there galaxies with $\beta_{star} \gg 1$ (UGC1230, UGC3137, UGC3371, UGC3851, UGC4173, UGC4278, UGC8286, UGC9211) and galaxies with $\beta_{star} < 1$ (UGC5721, UGC7524, UGC7603, UGC8837, UGC10310). Two systems (UGC1281 and UGC4325) have $\beta_{star} < 1$ but their 1σ confidence level are compatible with values $\gg 1$.

Noticeably the systems with the larger β_{star} are also the ones with the smaller stellar mass-to-light ratio. This is a warning for a possible degeneracy working among these two parameters. Such a degeneracy was already discussed in Paper I where we also noticed an anti–correlation between the Y_* and the only one β adopted. The fact that we have now broke down this latter in two coupling constant ensure us that β_{gas} is unaffected by any degeneracy, while β_{star} is not. This is a major benefit we have gained by the adoption of the mass component decoupling approach; we could add that the main coupling constant one should rely on is β_{gas}. Interestingly the gas status is really what it makes the big difference between cold and hot dynamical systems which correspondingly possess cold and hot gas.

Going more in details of the best fit stellar mass-to-light ratios, we have 11 of 15 galaxies compatible at 1σ level with the previously prescribed range; one (UGC7524) has an higher value; and three (UGC7603,UGC8286, UGC8837) have values smaller than 0.5. Among these, the first two were peculiar also in Paper I, even if being considered acceptable, and UGC7603 in particular still has the smallest value, $Y_* = 0.052$. Only in two cases (UGC4325 and UGC5721) we obtain more compatible values mainly due to their large errors. Anyway, in general, in Paper I we obtained a better match of Y_* with the prescribed range in 10 of 15 cases.

Finally, the interaction length shows a wider range than the clusters galaxies case not being very well constrained as in that case. One particular case being UGC3137: even in Paper I it was one of the galaxies with the largest interaction length, but now it has a too large value, $L \approx 500$ kpc, which is difficult to understand. Anyway, by taking a look to its rotational profile, we can see how it satisfies two main requirements: 1.

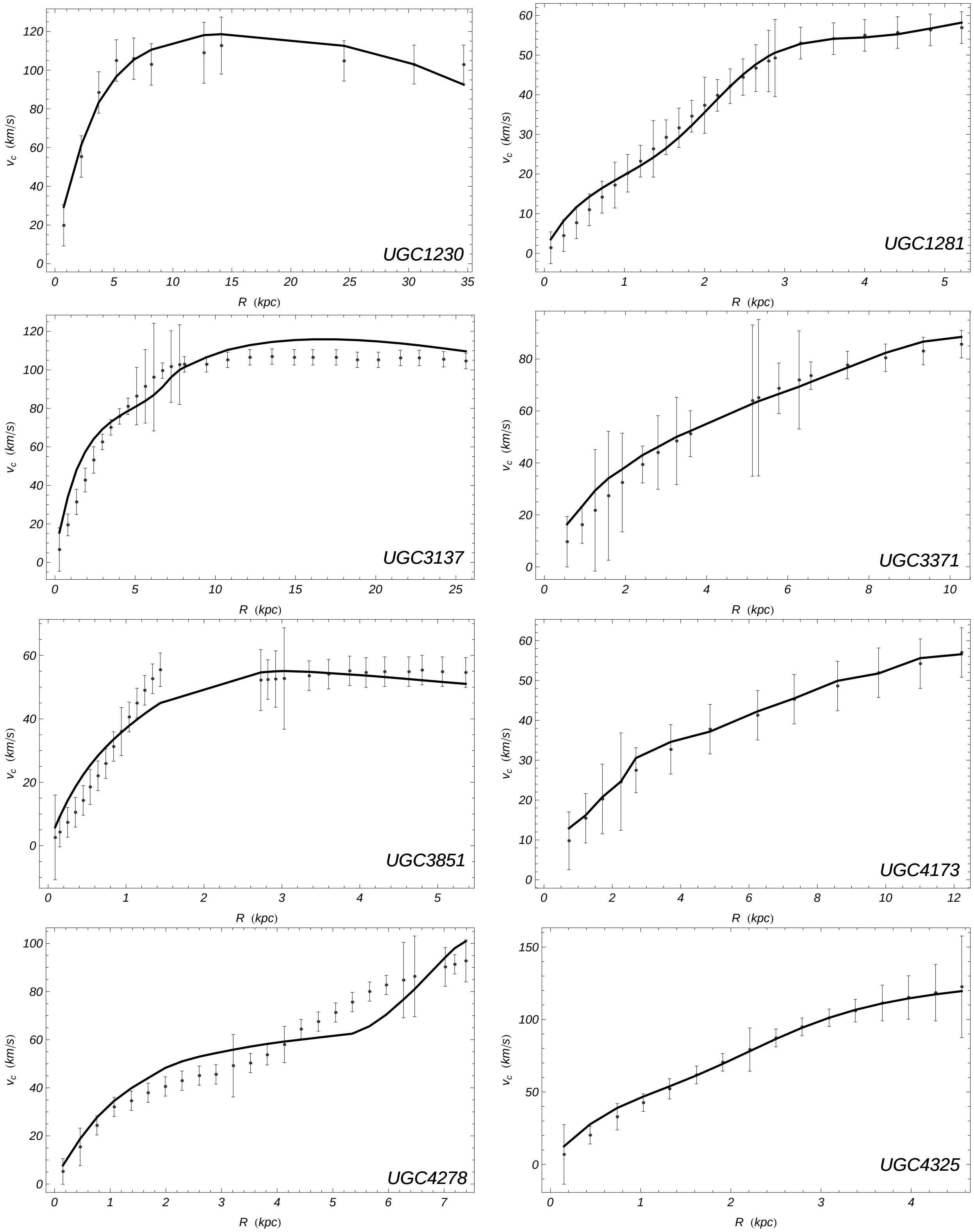

FIG. 8.— Rotation curves of LSB galaxies. Dots are velocities from data; solid line is the theoretical model, $v_c^2 = r\, d\Psi/dr$.

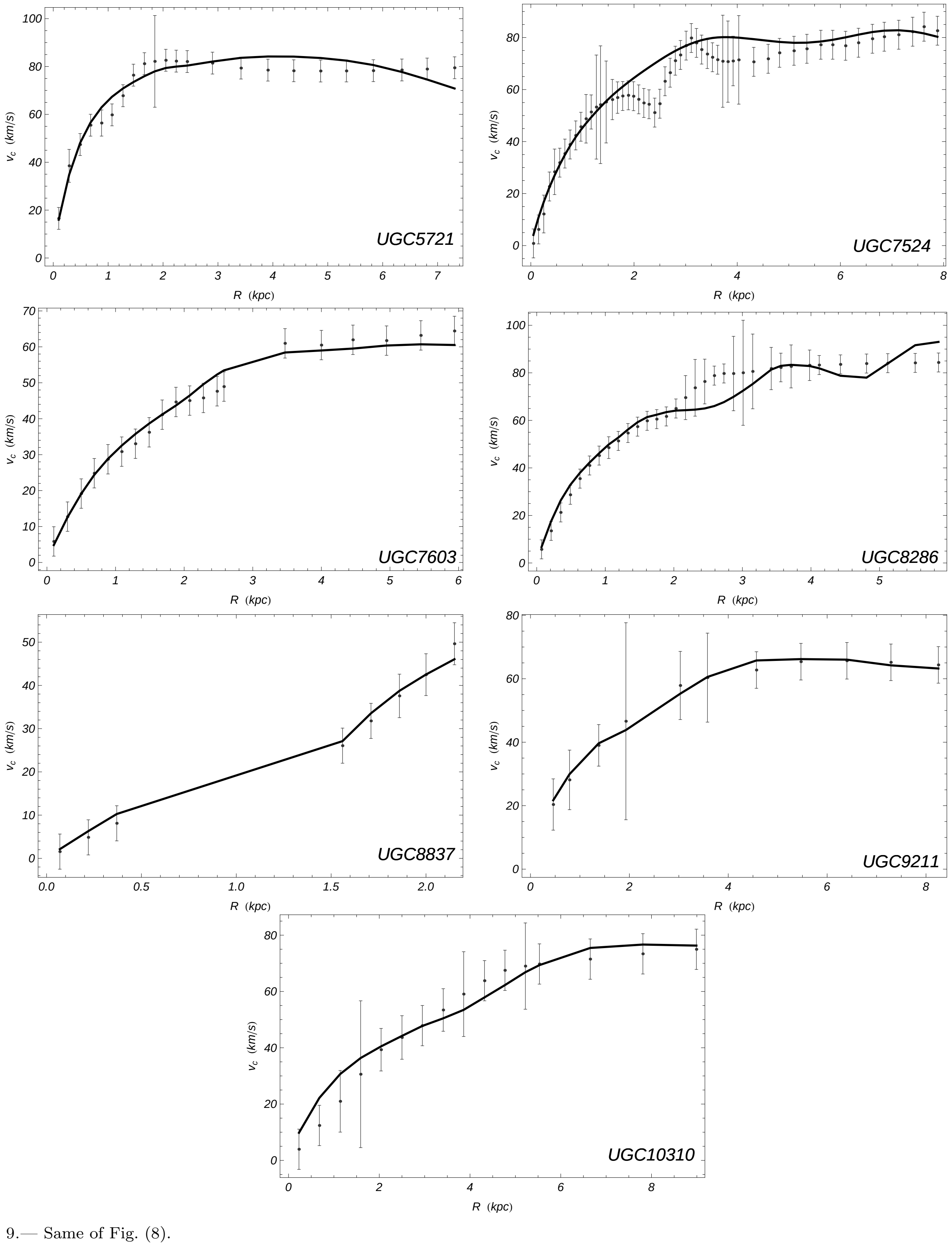

Fig. 9.— Same of Fig. (8).

it is the second largest object in the sample (or, better, the second object for which observations of the gas component where done up to a larger distance from the center); 2. it is the most clear case in which it seems to have reached the expected plateau in the rotation curve. Lacking more detailed, extended and less disturbed data for the galaxies in our sample we cannot conclude anything; we can only argue that in spiral galaxies, more than clusters and the elliptical galaxies, the degeneracy among parameters due to limited extension of the data could be more important.

As we did in Paper I, we search for possible scaling relations, also for comparing our alternative approach with more popular theories, like MOND (Swaters 2010).

A correlation among the gas coupling constant (probably more related to the global gravitational structure properties than the star related parameter) and the extrapolated central disk surface brightness $\mu_{0,R}$ (reported in Table 3 of Paper I) is possible, see top panel of Fig. 10:

$$\log \beta_{gas} = (-0.32 \pm 1.29) + (0.43 \pm 0.96) \cdot \log \mu_{0,R} \; ; \quad (40)$$

as long as between the same quantity and the maximum rotational velocity, see top panel of Fig. 11:

$$\log \beta_{gas} = (-0.30 \pm 0.28) + (0.30 \pm 0.14) \cdot \log V_{max} \; . \quad (41)$$

Excluding only peculiar cases with respect of β_{gas} (UGC3851, UGC4173, UGC4325, UGC5721) we can see that the dispersion around such relations is quite low. We also show in the top panel of Fig. 12 the relation between β_{gas} and the total gas mass of each galaxy:

$$\log \beta_{gas} = (0.20 \pm 0.06) + (0.04 \pm 0.04) \cdot \log M_{gas} \; ; \quad (42)$$

clearly the parameter is quite independent of such quantity, giving a further confirmation of our preliminary hypothesis $\mathrm{d}\beta/\mathrm{d}r \approx 0$. In the top panel of Fig. 13, we show the relation with the total baryonic (stars and gas) mass:

$$\log \beta_{gas} = (0.22 \pm 0.06) + (0.03 \pm 0.04) \cdot \log M_{bar} \; ; \quad (43)$$

We remind that in this case, in the estimation of the stellar counterpart, we have to take into account the stellar mass-to-light ration, Y_{*}, which is actually one of the fit parameters. No sensible changes are detected when moving from the gas to the total baryonic.

This does not happen when considering the coupling constant with stars; as it is possible that a degeneracy between the coupling constant and the stellar mass-to-light ratio is working, we consider more properly the quantity $\beta^2_{star} \cdot Y_{*}$ which appears in the stellar rotational contribution, finally having (bottom panel of Fig. 10):

$$\log \beta^2_{star} \cdot Y_{*} = (-11.69 \pm 1.71) + (9.01 \pm 1.28) \cdot \log \mu_{0,R} \; , \quad (44)$$

and (bottom panel of Fig. 11)

$$\log \beta^2_{star} \cdot Y_{*} = (1.45 \pm 2.44) + (-0.58 \pm 1.27) \cdot \log V_{max} \; , \quad (45)$$

which holds only for the galaxies with $\beta_{star} \gg 1$, while the others show a more scattered distribution.

The relation between $\beta^2_{star} \cdot Y_{*}$ and M_{gas} or M_{bar} are less evident than the previous case; taking a look to the bottom panels of Figs. 12 - 13 we can only detect (more clearly in the M_{bar} case) three sub-groups: two galaxies in the bottom-left corner (UGC7603 and UGC8837), corresponding to very low values for both β_{star} and Y_{*}; four galaxies in the middle (UGC1281, UGC4325, UGC5721 and UGC10310), corresponding to low values of β_{star}; and an almost constant $\beta^2_{star} \cdot Y_{*}$ group made of the remaining objects.

One the other side, the length parameter, L, does not show a clear ordered pattern when compared with the same quantities as before.

An even more interesting relation to be tested here is the well-known Baryonic Tully-Fisher (BTF) relation (McGaugh 2012), which relates the total baryonic mass of spiral galaxies, M_{bar}, with the maximum observed velocity, V_{max}, that in the outer regions becomes approximately flat, V_f and is actually quantified to be:

$$M_{bar} = A \cdot V_f^4 \; , \quad (46)$$

with $A = 47 \pm 6 \; M_{\odot} \; \mathrm{km}^{-4} \; s^4$. In order to make the comparison with our results more clear, we can re-write the previous in the equivalent expression:

$$\log V_f = (1.582 \pm 0.003) + 0.25 \log M_{bar} \; . \quad (47)$$

As it is possible to verify from previously plotted rotational curves, not all the galaxies in our sample seem to have reached the flatness regime in the rotational curve; so that the V_f appearing in the previous formulas is more exactly V_{max}, the maximum velocity evaluated at the maximum distance from the center available from the data.

In our alternative scenario, the total velocity can be written as the sum of different terms:

$$V_f^2 = V^2_{N,star} + V^2_{N,gas} + V^2_{C,star} + V^2_{C,gas} \; , \quad (48)$$

where the suffix N and C, ax explained in previous sections, are related to the (extended) Newtonian and corrective terms in our gravitational potential model.

If we first consider the quantity $V_{f,theo}$ made up with $V_{N,gas}$ entirely derived from direct velocity observations; $V_{N,star}$ mixing direct velocity observations and a fit parameter, Y_{*} (which also enters in the calculation of M_{bar}); and $V^2_{C,star}$ and $V^2_{C,gas}$ completely depending on our theoretical model, we obtain:

$$\log V_f = (1.558 \pm 0.030) + 0.25 \log M_{bar} \; , \quad (49)$$

which agree very well with the expected BTF relation. We can also check that the BTF relation is verified for any of the components of the total velocity (of course, we will consider the maximum velocity for any of these). For the pseudo-newtonian-term-derived stellar velocity we can identify two groups: galaxies with $Y_{*} > 2$ give

$$\log V_{N,star} = (0.547 \pm 0.067) + 0.25 \log M_{bar} \; , \quad (50)$$

and galaxies with $Y_{*} < 2$ give

$$\log V_{N,star} = (1.232 \pm 0.043) + 0.25 \log M_{bar} \; . \quad (51)$$

The pseudo-newtonian-term-derived gas velocity (excluding UGC4325) gives:

$$\log V_{N,gas} = (1.132 \pm 0.026) + 0.25 \log M_{bar} \; . \quad (52)$$

The corrective-term-derived stellar velocity (excluding UGC5721, UGC7603, UGC8837 and UGC10310) gives:

$$\log V_{C,gas} = (1.092 \pm 0.064) + 0.25 \log M_{bar} \; . \quad (53)$$

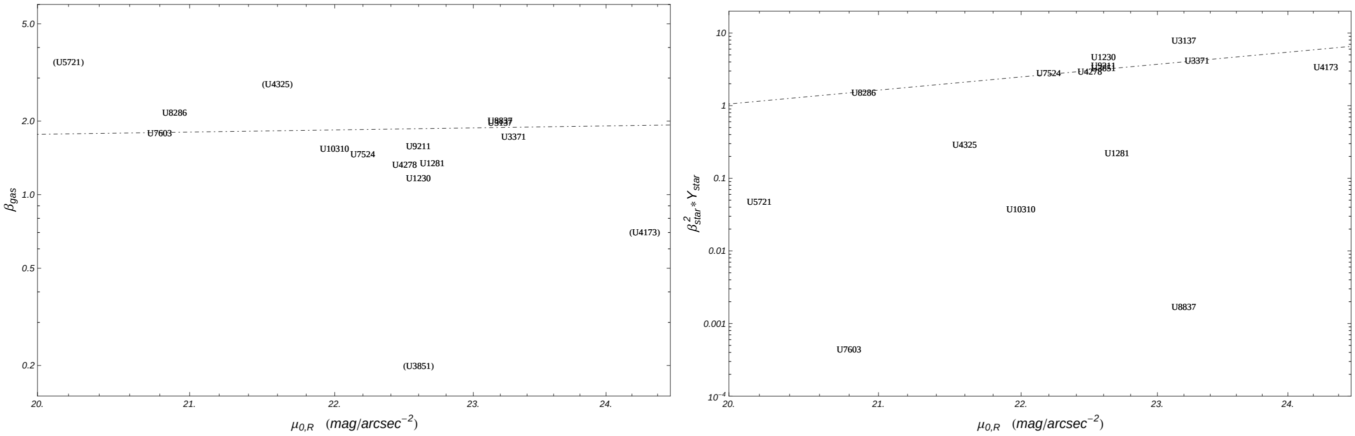

FIG. 10.— Correlation among the scalar field coupling constants and the central surface brightness of spiral galaxies.

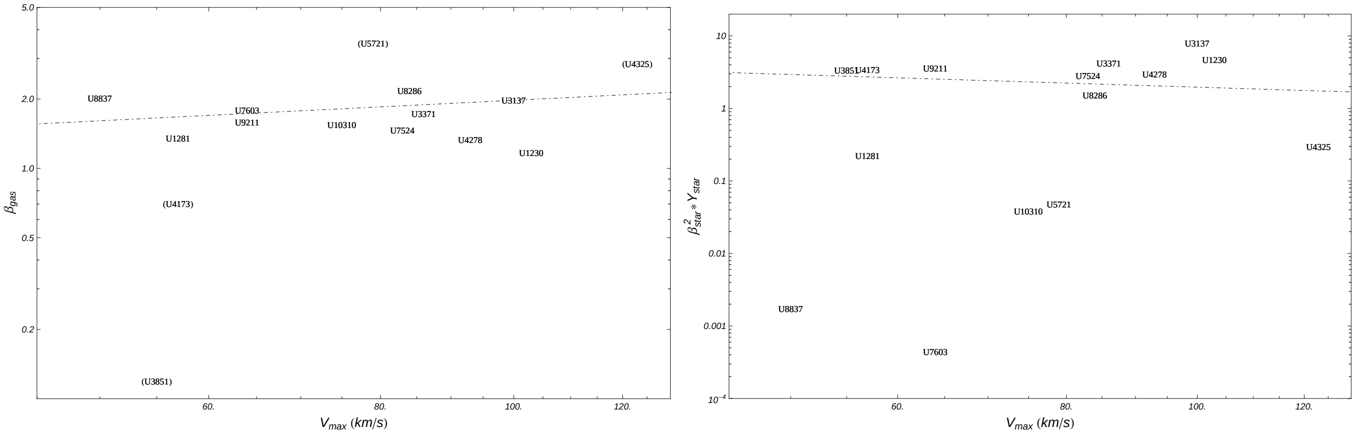

FIG. 11.— Correlation among scalar field coupling constants and the maximum stellar velocity.

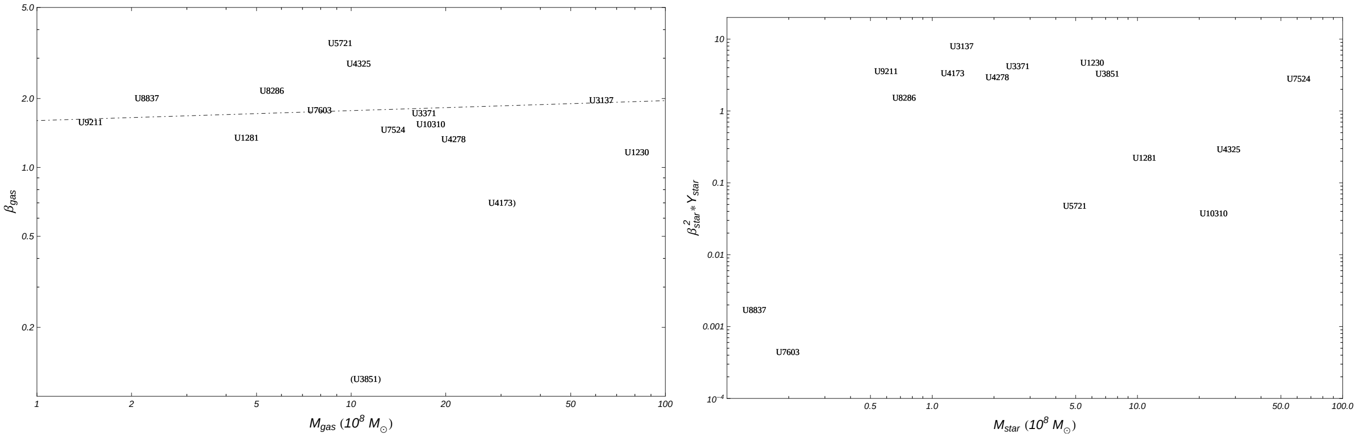

FIG. 12.— Correlation among scalar field coupling constants and the gas mass.

The corrective-term-derived gas velocity (excluding $UGC3851$) gives:

$$\log V_{C,star} = (1.448 \pm 0.051) + 0.25 \log M_{bar} \ . \qquad (54)$$

All the previous relations are in Figs. 14 - 15 It is interesting to note that, for these last two quantities, if we relax the condition for which the coefficient of M_{bar} has to be equal to 0.25, and we leave it free, we obtain, respectively, the values 0.037 and 0.033, which are quite consistent with a scenario where the contribution to the rotation curve coming from the effective mass produced by the modified gravity of the chosen scalar field is practically independent of the baryon mass (at least, for the family of spiral galaxies considered), so arguing in favor of a more universal task for our mechanism.

5.3. *Unified picture*

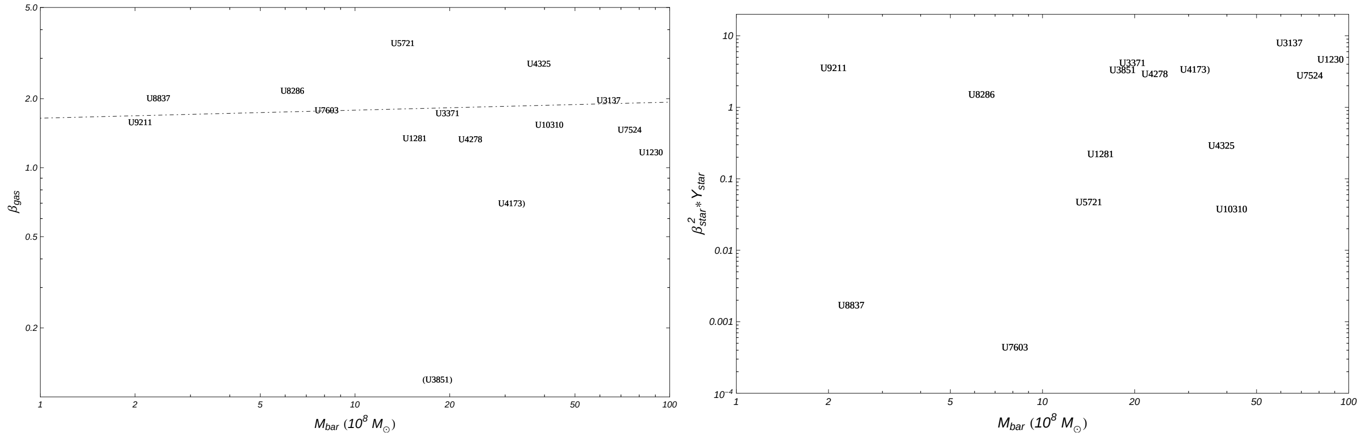

FIG. 13.— Correlation among scalar field coupling constants and the total baryonic mass.

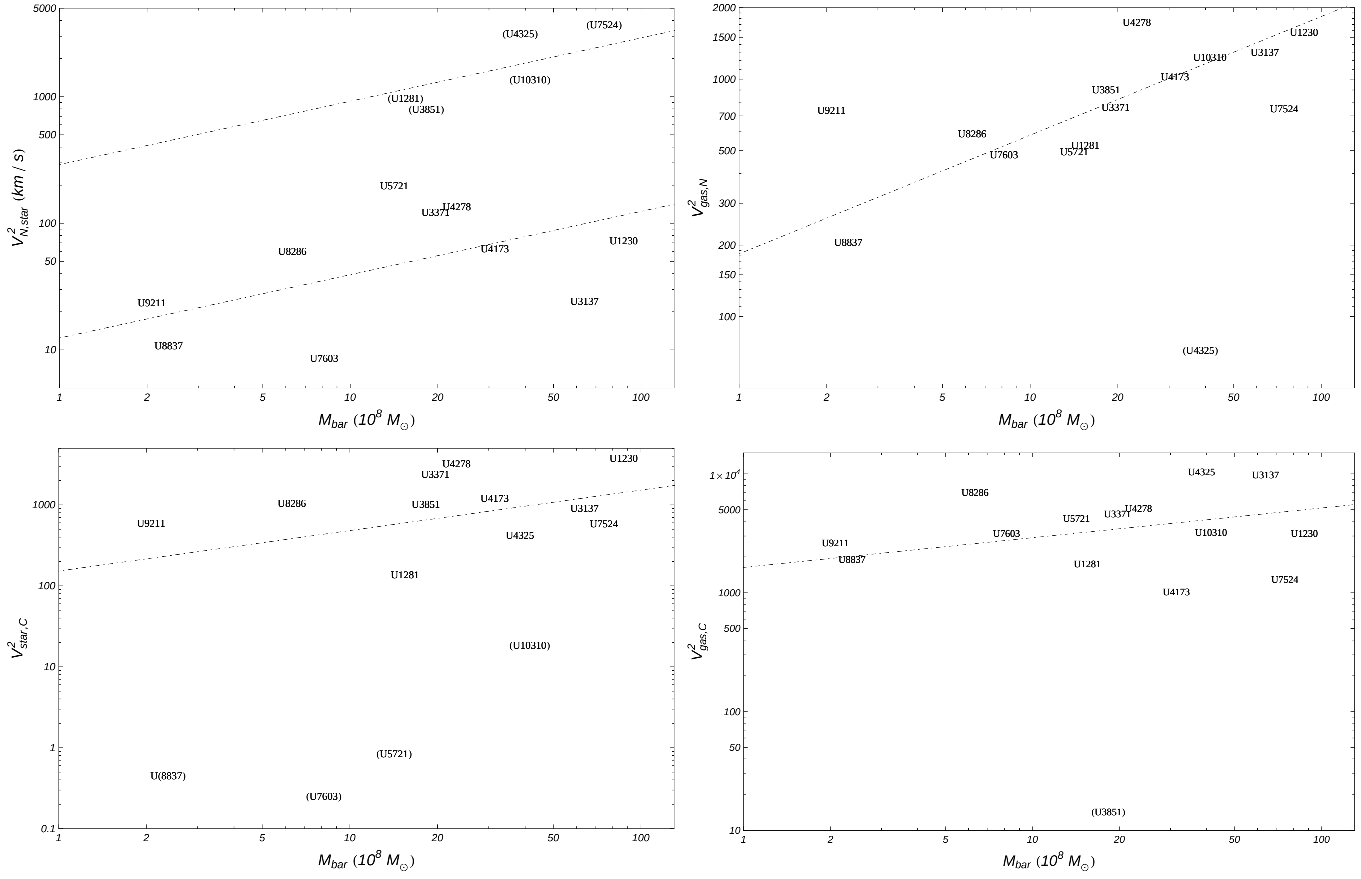

FIG. 14.— Baryonic Tully-Fisher relation for our galaxy sample: contributions from different velocity components.

In this section we will qualitatively draw some conclusions from the results that we have derived from the different gravitational structures discussed above. In particular we refer to the new evidence that a scalar field can mimic dark matter at different scales by changing its properties depending either on the local physical conditions, namely the matter density, or the matter status.

As done in Paper I, we consider the relation among the scalar field parameters and the gas density/mass of any structure in order to check the presence of a global correlation among parameters at all scales, from galaxies to galaxy clusters.

For galaxy clusters this is natural to check because the gas is the main contribution to the mass (under the assumption that there is no dark matter, as in the current work). The same argument it is not intuitive for galaxies, as gas is not the main component at galactic scale: however as we have found that the coupling constant of the gas with the scalar field can be larger than the one of stars, this component turns out to have a significant impact on the observational quantities too, sometimes even larger than the stellar one.

Let us start by verifying how the scalar field parameters are correlated with each other. We remind that one

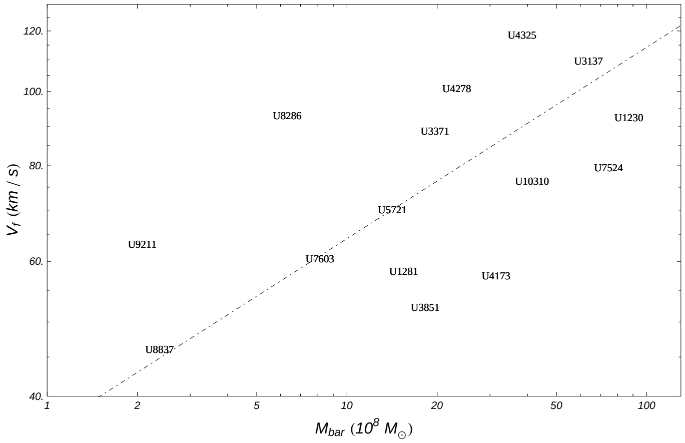

FIG. 15.— Baryonic Tully-Fisher relation for our galaxy sample: total rotational velocity.

of our main hypothesis is that the coupling constants β are independent of the scale or, more precisely, that $d\beta/dr \sim 0$. We can verify a posteriori that this hypothesis is quite well satisfied by taking a look to the top pane of Fig. 16. Here a linear regression of the spiral galaxy parameters gives:

$$\log \beta_{gas} = (0.19 \pm 0.05) + (0.04 \pm 0.02) \cdot \log L \ ; \quad (55)$$

while for clusters of galaxies we obtain:

$$\log \beta_{gas} = (0.91 \pm 0.18) - (0.17 \pm 0.06) \cdot \log L \ ; \quad (56)$$

and using all data together we finally get:

$$\log \beta_{gas} = (0.20 \pm 0.05) + (0.06 \pm 0.02) \cdot \log L \ . \quad (57)$$

We can verify how coherently each gravitational structure family locate in the parameter space: the clusters of galaxies lay in a very well constrained region on the right side of top panel in Fig. 16; spiral galaxies are on the opposite side with a larger dispersion mainly due to the uncertainties on the interaction length. The only elliptical galaxy that we have analyzed is interestingly located right in between the spirals and the galaxy cluster regions very close to the area where the smallest clusters and/or group of galaxies are located. This evidence seems to suggest that the properties of the scalar field are related to the dynamical properties of the gravitational systems, as cold dynamical systems like spirals are clearly separated by hot dynamical systems (elliptical galaxies and galaxy clusters). This result is interesting as the connection between dynamics (especially anisotropy of the orbits) and scalar field parameters has been found also in other $f(r)$ formulations (Napolitano et al. 2012).

For the coupling constant related to stars (in galaxies) and galaxies (in clusters), in the bottom panel of Fig. 16 we can see a larger dispersion in the parameter space, but also a clear segregation: the left half of the diagram is dominated by spiral galaxies, the right half by clusters of galaxies, and the central region populated by elliptical galaxies (although a larger sample is required) and smaller clusters and/or group of galaxies.

We can eventually reach the same conclusion looking at the correlation between scalar field parameters and the gas density as in Fig. 17: when considering the top and middle panels of this figure we can see that the parameters do not distribute randomly, but seem to follow a trend. For the interaction length, the top left corner is populated by clusters of galaxies, the bottom right by spiral galaxies, and the center possibly by elliptical galaxies and group of galaxies, with a clear linear trend and a dispersion which is larger for spiral galaxies than for clusters. A linear regression in the log-log space where the interaction length L is the dependent variable give, for spiral galaxies:

$$\log L = (10.29 \pm 4.68) - (1.87 \pm 0.96) \cdot \log \rho_{gas} \ ; \quad (58)$$

for clusters of galaxies:

$$\log L = (5.94 \pm 1.37) - (0.78 \pm 0.35) \cdot \log \rho_{gas} \ ; \quad (59)$$

and for all systems together:

$$\log L = (9.67 \pm 1.04) - (1.74 \pm 0.23) \cdot \log \rho_{gas} \ . \quad (60)$$

For the gas coupling constant, on the other side, we have a linear trend almost compatible with a constant β_{gas}, thus confirming our previous hypothesis ($\mathrm{d}\beta/\mathrm{d}r \approx 0$); in particular for spiral galaxies we have:

$$\log \beta_{gas} = (-0.31 \pm 0.57) + (0.11 \pm 0.12) \cdot \log \rho_{gas} \ ; \quad (61)$$

for clusters of galaxies we have:

$$\log \beta_{gas} = (-0.04 \pm 0.41) - (0.11 \pm 0.10) \cdot \log \rho_{gas} \ ; \quad (62)$$

end for the total sample:

$$\log \beta_{gas} = (1.01 \pm 0.18) - (0.16 \pm 0.04) \cdot \log \rho_{gas} \ . \quad (63)$$

When considering the combination of β_{star} and Y_* or β_{gal}, the large spread does not allow to define a clear trend and no data regression is produced.

6. A CONSISTENCY CHECK: STRONG LENSING CONVERGENCE MAP

In previous sections we have extensively tested the dynamical effects of the scalar field theories against the stellar dynamics of elliptical galaxies, the gas kinematic of spiral systems and the hydrostatical equilibrium of galaxy clusters. We have shown that the modified potential as in Eq. 4 has successfully passed all these astrophysical tests by carefully taking care of the coupling with the different baryonic mass components of the gravitating systems (i.e. stars and gas). Most of these tests rely, though, on classical mechanics and

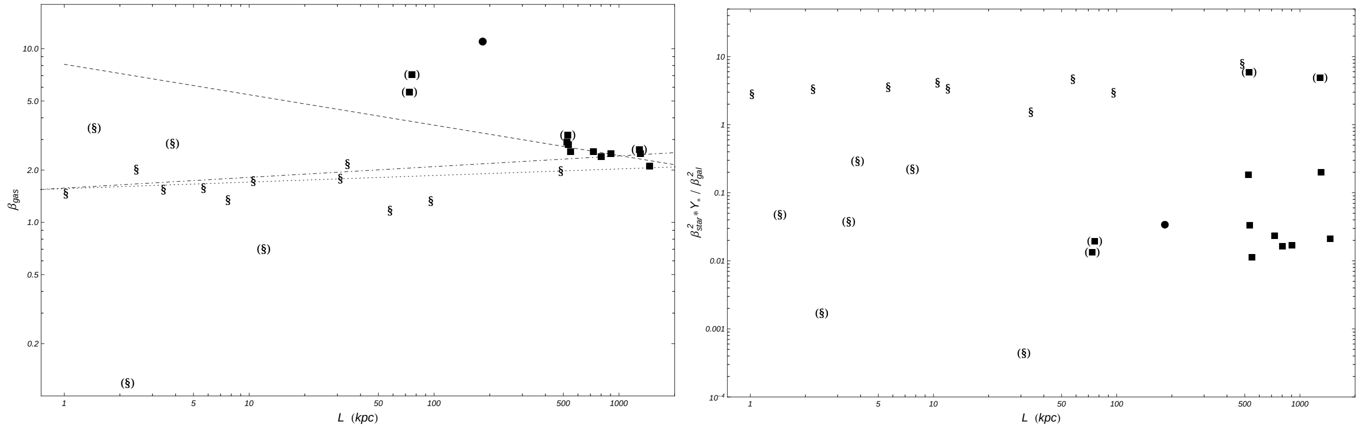

FIG. 16.— Correlation among the scalar field parameters: spirals are LSB spiral galaxies; filled squares are clusters of galaxies; filled circle is the elliptical galaxy NGC4374. Dashed line is the best fit for clusters only; dotted line is the best fit for spiral galaxies only; dot-dashed line is the best fit for the total sample. Objects in brackets are the peculiar cases described in the text and not considered in the fits.

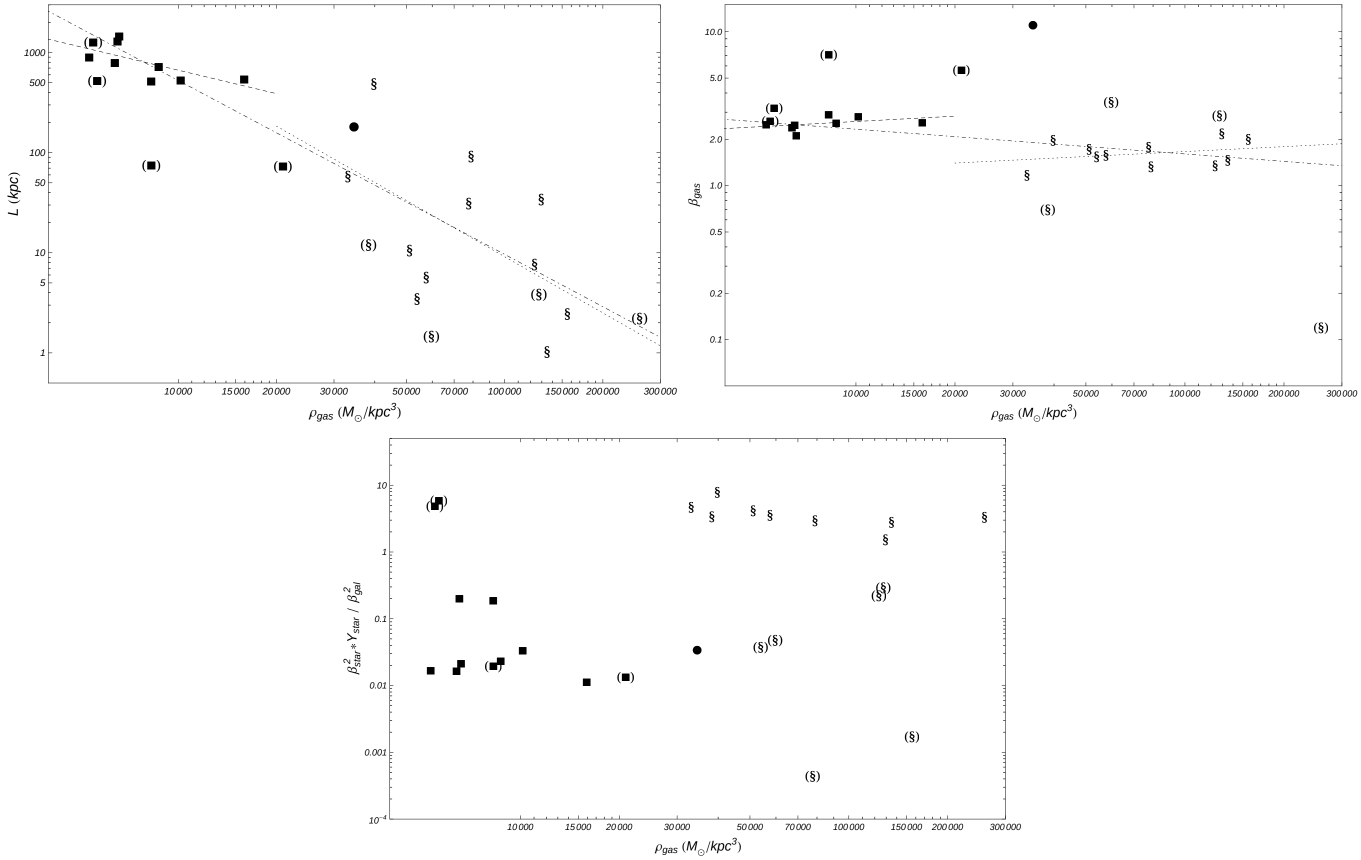

FIG. 17.— Correlation among the scalar field parameters and the gas density: spirals are LSB spiral galaxies; filled squares are clusters of galaxies; filled circle is the elliptical galaxy NGC4374. Dashed line is the best fit for clusters only; dotted line is the best fit for spiral galaxies only; dot-dashed line is the best fit for the total sample. Objects in brackets are the peculiar cases described in the text and not considered in the fits.

hydrostatic equilibrium (i.e. they imply all the same kind of physics). One can ask whether the gravitational effects produced by the scalar field potential can be equally effective in reproducing lensing observations, which have to be interpreted within general relativity. This is a natural passage for any alternative or extended theories of gravity (Bruneton & Esposito-Farese 2007; Angus et al. 2006; Feix et al. 2008, 2010; Lubini et al. 2011; Bernal et al. 2011; Brownstein & Moffat 2007) as a failure on accounting for lensing measurements is a too strong flaw for a theory to stay stand.

A complete and exhaustive treatment of gravitational lensing predictions and modeling will be presented in a forthcoming paper. Here we want to present a simple test to visualize whether the proposed approach is suitable to extend the scalar field gravity to lensing analyses.

Due to its intrinsic properties (i.e. the existence of different coupling constants with different kind of matter) we anticipate that the lensing test might present some difficulties from the observational point of view. We remind that the source of the total potential is given by the surface density distribution of baryons (galaxies and gas in this case) which in many cluster can be rather noisy (e.g. too few cluster members and/or low X-ray emission signal-to-noise ratio). As seen for elliptical galaxie, also for cluster there are currently not so many systems on the market for which it is possible to have high quality data from both spectroscopy (i.e., redshift) and X-ray gas emissions along with reliable strong and/or weak lensing features at the same time.

As a preliminary test we have performed the strong lensing analysis of A383, one of the clusters involved in our X-rays analysis as in § 5.1. This cluster is particular suitable for our purpose as there are literature measurements for high resolution data for X-ray gas (as explained in the related section here and in Paper I) and recent observations from the Cluster Lensing And Supernovae survey with Hubble–*CLASH* project (Postman et al. 2011) which have produced accurate strong (Zitrin et al. 2011, Z+11 hereafter) and weak lensing maps (Zitrin et al. 2012). In particular, we have been provided of strong lensing convergence (κ) map from Z+11 (see their Fig. 4), obtained under the standard dark matter paradigm, which we have compared against the prediction of the scalar field theory. The Z+11 $\kappa-$map is obtained from the multiple-image systems attributed to a galaxy candidate locate at redshift $z_s = 2.55$ (the redshift of A383 is $z_l = 0.189$). According to the the standard strong lensing equations in Newtonian gravity, the two dimensional surface mass distribution is related to the lensing-observable quantity, the convergence κ (Schneider et al. 1992). This relation writes (Peacock 2003):

$$\kappa(x,y) = \int \frac{4\pi G_N}{c^2}\frac{D_l D_{ls}}{D_s}\rho(x,y,z)\mathrm{d}z \equiv \frac{\Sigma}{\Sigma_c}\ , \qquad (64)$$

where

$$\Sigma(x,y) = \int \rho(x,y,z)\mathrm{d}z\ , \qquad (65)$$

is the two dimensional surface mass density and

$$\Sigma_c = \frac{c^2}{4\pi G_N}\frac{D_s}{D_l D_{ls}}\ , \qquad (66)$$

is the Newtonian critical surface mass density, D_s is the angular diameter distance to the background source galaxy, D_l is the angular diameter distance to the lens and D_{ls} is the angular diameter distance between the lens and the source. All distances are calculated given the source and lens redshift, and the fiducial cosmological model with $\Omega_m = 0.3$, $\Omega_\Lambda = 0.7$ and $h = 0.7$.

In an alternative scenario, we can modify the previous formula (Brownstein & Moffat 2007) in:

$$\kappa(x,y) = \int \frac{4\pi G(r)}{c^2}\frac{D_l D_{ls}}{D_s}\rho(x,y,z)\mathrm{d}z \equiv \frac{\overline{\Sigma}(x,y)}{\Sigma_c}\ , \qquad (67)$$

where

$$\overline{\Sigma}(x,y) = \int \mathcal{G}(r)\rho(x,y,z)\mathrm{d}z\ , \qquad (68)$$

is the weighted surface mass density, now not only related to the mass distribution, but also to the (alternative) gravity theory through the modified gravitational constant given in our case by:

$$\mathcal{G} = \frac{G(r)}{G_N} = 1 + 2\beta^2\exp(-r/L)\left(1+\frac{r}{L}\right)\ . \qquad (69)$$

Following the same approach of previous sections, we have now that the mass density $\rho(x,y,z)$ is made only of the baryonic components (gas and galaxies), and that the scalar field can couple with each of them with different strength.

The κ-map from Z+11 is reproduced as light contours in our Fig. 18 where we also overplot the derivation of the convergence map from our theoretical model using Eqs. 67 - 69 as black contours. This model, which best approximates the original map from Z+11, corresponds to $\beta_{gas} \sim 2.98$, $\beta_{gal} \sim 0.8$ and $L \sim 590$ kpc in Eq. 69.

The visual inspection of the map derived in our scalar field gravity clearly shows the over-simplification of the approach, as the derived $\kappa-$map is spherically symmetric while in the Z+11 map the map takes into account the local contribution of the massive galaxies in the field which perturb the overall convergence of the cluster potential. This causes a disagreement of the iso$-\kappa$ contours in many points, e.g. along the South-West direction , where the fairly round behavior of observationally reconstructed mass model is partially broken.

Overall, despite the simple analysis, our model seems to recover the main features of the Z+11 map with the all the iso$-\kappa$ contours overlapping each other for large portions, thus showing a fair correspondence between all the plotted mass density level. This is better quantified by the 1$-$dimension $\kappa-$map in Fig. 18 (right) obtained by dividing the surface mass estimations both from data and our model in radial bins of 10 kpc. As it can be easily seen, the agreement is very good which shows that the scalar field potential is compatible also with lensing data for A383.

Importantly, the parameter values which allowed the best match to data turned out to be overall compatible with the ones derived from the X–ray analysis as in Table 4, although there are some slight differences. E.g., the coupling with galaxies, β_{gal}, is slightly higher than the value derived from the X-ray reconstructed mass analysis, but this is not unexpected, as X-ray data are less trustworthy in the very inner region of clusters, i.e., for $R < 70$ kpc, where out-of-virial-equilibrium phenomena (cooling flow) can alter the results.

It is also possible that this lensing vs. X–rays discrepancies can be ascribed to the typical discrepancy found also under the dark matter paradigm (see e.g. Comerford & Natarajan 2007) which might be possibly related to intrinsic inconsistency of the technique assumptions rather than being physical (e.g. Sereno 2007).

In summary, we think that this preliminary test reasonably shows that our alternative model can be compatible with gravitational lensing. Future steps to improve the lensing analysis will include: *i*) a full theoretical analysis of gravitational lensing in our alternative scenario; *ii*) the use of a larger sample of galaxy clusters by combining X-ray observation and gravitational lensing (where possible) in a more self-consistent way; *iii*) the inclusion of the single galaxies contribution in the same fashion of lensing reconstruction models, in order to break the spherical symmetry and to obtain an even better agreement with data; *iv*) the extension of the analysis also to the weak lensing.

7. CONCLUSIONS AND DISCUSSION

In this work we have investigated the dynamical properties of several astrophysical systems, from galaxies to cluster of galaxies, within the theoretical framework of scalar-tensor theories as alternative to the dark matter paradigm, and looked for observational signatures in galaxy kinematics, X–ray equilibrium and gravitational lensing.

The crucial ingredients of our work are some novel properties of the scalar field with respect to previous analyses (Paper I): (i) a new parametrization of the theory where we have introduced the coupling of the scalar field with the different baryon component of the gravitational systems (stars and gas) and (ii) its mass (or interaction length) can vary with scale.

This new parametrization with basically two coupling constants, provided allowed the scalar field to mimic dark matter, i.e. by reproducing remarkably well observations without introducing a new kind of matter and by a modification of gravity.

Going in more details of the results in the different astrophysical test we have performed here, results have shown that (i) the velocity dispersion of elliptical galaxies can be fit very well by a scalar field, even better than assuming a classical Navarro-Frenk-White profile for the dark matter component; (ii) a scalar field can fairly well reproduce the matter profile in clusters of galaxies, estimated by X-ray observations and without the need for any additional dark matter; (iii) good fits to the rotation curves of low surface brightness galaxies are obtained. We have finally performed a preliminary test of the modified potential derived in the scalar field gravity to reproduce strong lensing convergence map of one of the X-ray clusters in our sample. Despite the simplified approach adopted, we have obtained a nice match of the $\kappa-$map with the one obtained from a detailed standard DM analysis from Z+11.

All these results show that scalar field gravity theories can be compatible with a wide range of astrophysical testa and can be considered as a viable alternative to the dark matter. In particular, our results show the possibility that the scalar field can couple with ordinary matter with different strength (different coupling constants) depending on the clustering state of matter components in the considered gravitational structures and that a possible correlation with the evolutionary state of gravitational systems is possible.

We point out that this is only the first of a longer series of works where we are intended to test our model and parametrization by using other different cosmological and astrophysical probes. In future works, on the cosmological side, we will study the feasibility of this model with the cosmic microwave background radiation data and matter power spectrum features; while, on the astrophysical side, we will explore the possible correlations between classical models (NFW or generalized NFW profiles) for dark matter and the effective contribution from our scalar field; for what it concerns spiral galaxies, it will be interesting to verify if and how our model is able to reproduce the Universal Rotation Curve scenario (Persic et al. 1997; Salucci 2011). Even more decisive will be to test the model with the gravitational lensing phenomenon. This is a major probe to rule out modified gravity alternatives to dark matter, such as non-relativistic MOND (Bruneton & Esposito-Farese 2007), or to put constraints on other models such as TeVeS by requiring the existence of massive neutrinos (Angus et al. 2006; Feix et al. 2008, 2010). Since our model is not a subclass of MOND/TeVeS or the standard scalar-tensor theories, it is not ruled out by lensing observations. In fact, the model studied here, is more similar from the theoretical point of view, to the ones studied in (Lubini et al. 2011; Bernal et al. 2011; Brownstein & Moffat 2007), where the authors show that all the gravitational predictions obtained in general relativity are still valid in alternative theories like chameleon-$f(R)$-gravities. Due to these reasons we have already planned a detailed analysis of strong and weak lensing applied to clusters of galaxies, and we believe that the possibility of decoupling the different baryonic mass component in a gravitational structure, with different coupling constant with the chosen scalar field, can make us to recover gravitational lensing observations and without the need of any massive neutrinos component.

ACKNOWLEDGMENTS

D.F.M. thanks the Research Council of Norway FRINAT grant 197251/V30. D.F.M. is also partially supported by project PTDC/FIS/111725/2009 and CERN/FP/123618/2010. V. S. is now working at UPV/EHU under the project "Gravitación, Cosmologiá Relativista y otros aspectos de la Estructura del Universo". S. C. acknowledges the support of INFN (Sez. di Napoli) and the ERASMUS/SOCRATES European program. V.S. thanks A. Zitrin for providing data from lensing, L. Coccato for giving important suggestions in managing elliptical galaxies data, Y. Fukazawa for providing data about X-ray emission of NGC4374 and P. Brownstein for giving interesting comments and suggestions.

REFERENCES

Acquaviva, V., Baccigalupi, C., Leach, S.M., Liddle, A.R., Perrotta, F., 2005, Phys. Rev. D, 71, 104025
Angus, G.W., Famaey, B., Zhao, H. S., 2006, MNRAS, 371, 138
Bekenstein, J. D., 2004, Phys. Rev. D, 70, 083509
Bergond, G., Zepf, S.E., Romanowsky, A.J., Sharples, R.M., Rhode, K.L., 2006, A&A, 448, 155
Bertone, G., Hooper, D., Silk, J., 2005, Phys. Rept., 405, 279
Bernal, T., Capozziello, S., Hidalgo, J.C., Mendoza, S., 2011, Eur. Phys. J. C 71, 1794
Bertschinger, E., Zukin, P., 2008, Phys. Rev. D, 78, 024015
Binetruy P., 2006, Supersymmetry: Theory, experiment and cosmology, *Oxford, UK: Oxford Univ. Pr. 520 p*
Brax, P., van de Bruck, C., Davis, A.-C., Khoury, J., Weltman, A., 2004, Phys. Rev. D, 70, 123518
Brax. P., et al., 2012, accepted to JCAP
Brownstein, J.R., Moffat, J.W., 2007, MNRAS, 382, 29
Bruneton, J. P., Esposito-Farese, G., 2007, Phys. Rev. D, 76, 124012
Bryan, G.L., ApJ, 495, 80
Buote, D.A., Humphrey, P.J., 2011, arXiv:1104.0012
Capaccioli, M., Caon, N., D'Onofrio, M., 1992, MNRAS, 259, 323

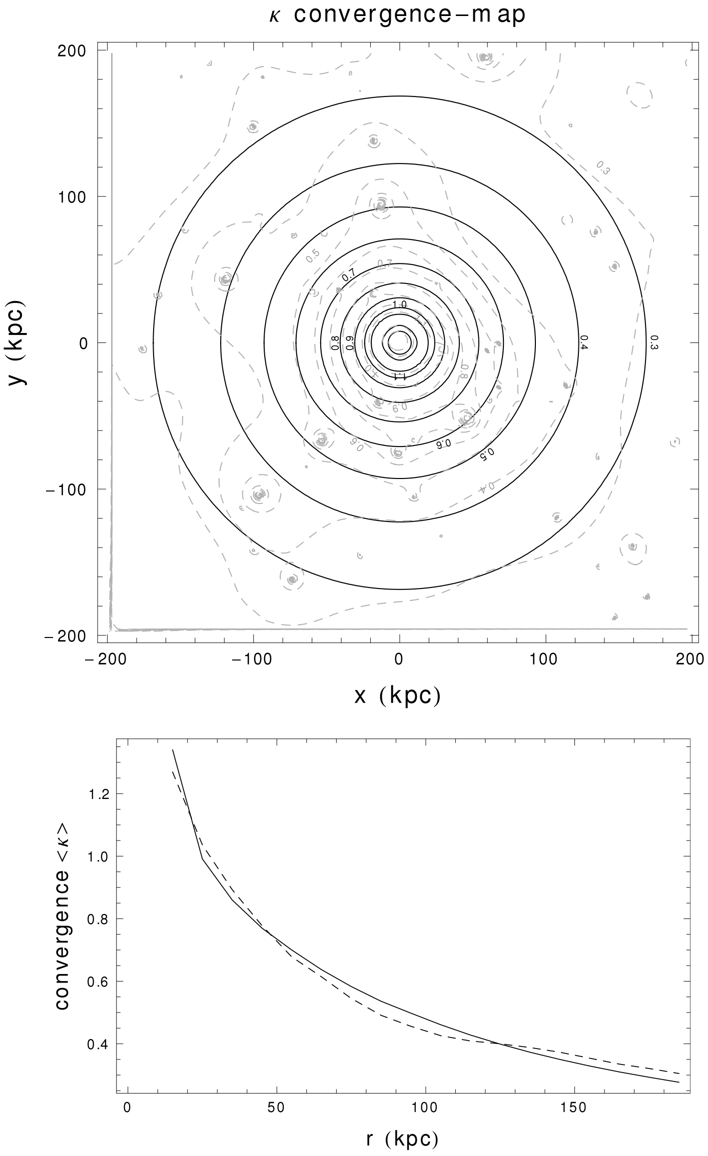

Fig. 18.— Top: 2D surface mass distribution (κ), in units of the critical density (for a source located at $z_s = 2.55$), of A383. North is up, East is left. Contours are in linear units; grey contours are from observational data in (Zitrin et al. 2011); black ones are from our scalar field model. Bottom: Radial surface mass density (κ) profile in units of the critical surface density (for a source located at $z_s = 2.55$), of A383. To be compared with Fig. 5 of (Zitrin et al. 2011). The dashed line is from observational data in (Zitrin et al. 2011); the solid one is from our scalar field model.

Capozziello, S., 2002, Int. Jou. Mod. Phys., D 11, 483

Capozziello, S., Carloni, S., Troisi, A., 2003, Recent Res. Dev. Astron. Astrophys. **1**, 625

Capozziello, S. and Tsujikawa, S., 2008, Phys. Rev. D 77, 107501

Capozziello, S. and Francaviglia, M., 2008, Gen. Rel. Grav., 40, 357

Capozziello, S. and De Laurentis, M., 2011, Phys. Repts., 509, 167

Cappellari, M., et al., 2006, MNRAS, 366, 1126

Carroll, S.M., Press, W.H., Turner, E.L. 1992, ARA&A, 30, 499

Cavaliere, A., Fusco-Femiano, R., 1978, A&A, 70, 677

Clifton, T., Mota, D., Barrow, J., 2005, Mon. Not. R. Astron. Soc., 358, 601

Coccato, L., Gerhard, O., Arnaboldi, M., Das, P., Douglas, N.G., Kuijken, K., Merrifield, M.R., Napolitano, N.R., Noordermeer, E., Romanowsky, A.J., Capaccioli, M., Cortesi, A., De Lorenzi, F., Freeman, K.C., 2009, MNRAS, 394, 1249

Copeland E.J., Sami M., Tsujikawa S., 2006, Int. J. Mod. Phys. D 15, 1753

Davis et al., arXiv:1108.3081 [astro-ph.CO]

Dekel, A., Stoehr, F., Mamon, G.A., Cox, T.J., Novak, G.S., Primack, J.R., 2005, Nature, 437, 707

de Blok, W.J.G., Bosma, A., 2002, A&A, 385, 816

De Lorenzi, F., Gerhard, O., Saglia, R.P., Sambhus, N., Debattista, V.P., Pannella, M., Méndez, R.H., 2008, MNRAS, 385, 1729

Diehl, S., Statler, T.S., 2007, ApJ, 668, 150

Douglas, N.G., Arnaboldi, M., Freeman, K.C., Kuijken, K., Merrifield, M.R., Romanowsky, A.J., Taylor, K., Capaccioli, M., Axelrod, T., Gilmozzi, R., Hart, J., Bloxham, G., Jones, D., 2002, PASP, 114, 1234

Douglas, N.G., 2007, ApJ, 664, 257

Dunkley, J., Bucher, M., Ferreira, P. G., Moodley, K., Skordis, C., 2005, MNRAS, 356, 925

Esposito-Farese, G., Polarski, D., Phys. Rev. D, 63, 2001, 063504

Evrard, A.E., Metzler, C.A., Navarro, J.F., 1996, ApJ, 469-494

Feix, M., Fedeli, C., Bartelmann, M., 2008, A&A, 480, 313

Feix, M., Zhao, H., Fedeli, C., Pestaña Garrido, J. L., Hoekstra, H., 2010, Phys. Rev. D, 82, 124003

Fukazawa, Y., Betoya-Nonesa, J.G., Pu, J., Ohto, A., Kawano, N., 2006, ApJ, 636, 698

Gannouji, R., Moraes, B., Polarski, D., arXiv:0907.0393

Gultekin, K., Richstone, D.O., Gebhardt, K., Lauer, T.R., Tremaine, S., Aller, M.C., Bender, R., Dressler, A., Faber, S.M., Filippenko, A.I., Green., R., Ho, L.C., Kormendy, J., Magorrian, J., Pinkney, J., and Siopis, C., 2009, ApJ, 698, 198

TABLE 4

Clusters of galaxies: Scalar field. COLUMN 1: NAME OF THE CLUSTER. COLUMN 2: COUPLING CONSTANT OF SCALAR FIELD AND GALAXY COMPONENT. COLUMN 3: COUPLING CONSTANT OF SCALAR FIELD AND GAS COMPONENT. COLUMNS 4: SCALAR FIELD INTERACTION LENGTH.

	β_{gal}	β_{gas}	L (kpc)
A133	$2.230^{+0.778}_{-1.080}$	$2.645^{+0.202}_{-0.212}$	$1289.18^{+145.62}_{-188.13}$
A262	$0.117^{+0.308}_{-0.086}$	$5.687^{+1.719}_{-1.099}$	$73.628^{+33.572}_{-22.954}$
A383	$0.107^{+0.337}_{-0.079}$	$2.584^{+0.106}_{-0.125}$	$547.703^{+84.917}_{-50.069}$
A478	$0.129^{+0.415}_{-0.097}$	$2.410^{+0.214}_{-0.165}$	$802.668^{+292.035}_{-205.815}$
A907	$0.435^{+3.472}_{-0.377}$	$2.922^{+0.254}_{-2.500}$	$523.430^{+693.474}_{-78.797}$
A1413	$0.452^{+0.830}_{-0.390}$	$2.501^{+0.064}_{-0.096}$	$1305.87^{+76.33}_{-83.37}$
A1795	$0.154^{+0.532}_{-0.118}$	$2.568^{+0.207}_{-0.198}$	$727.922^{+389.727}_{-174.47}$
A1991	$0.184^{+0.635}_{-0.145}$	$2.823^{+0.144}_{-0.138}$	$532.531^{+76.564}_{-33.074}$
A2029	$0.131^{+0.473}_{-0.096}$	$2.516^{+0.210}_{-0.180}$	$905.584^{+275.600}_{-271.873}$
A2390	$0.147^{+0.390}_{-0.105}$	$2.123^{+0.076}_{-0.083}$	$1465.02^{+94.02}_{-104.32}$
MKW4	$0.141^{+0.449}_{-0.106}$	$7.169^{+2.554}_{-1.566}$	$75.932^{+36.494}_{-25.118}$
RXJ1159	$2.454^{+0.355}_{-0.273}$	$3.206^{+0.124}_{-0.162}$	$528.456^{+45.442}_{-27.393}$

Hinterbichler, K., Khoury, J. 2010, Physical Review Letters, 104, 231301

W. Hu, I. Sawicki, Phys. Rev. **D76**, 064004 (2007).

Humphrey, P.J., Buote, D.A., Gastaldello, F., Zappacosta, L., Bullock, J.S., Brighenti, F., Mathews, W.G., 2006, ApJ, 646, 899

Jing, Y.P., Suto, Y., 2000, ApJ, 529, L69

Khoury, J., Weltman, A., 2004, Phys. Rev. D, 69, 044026

Klypin, A., Prada, F., 2009, ApJ, 690, 1488

Koivisto T., Mota D. F., Phys. Rev. 2006, D73, 083502.

Koivisto, T. S., Mota D. F., Pitrou C., 2009, JHEP 0909, 092.

Kormendy, J., Fisher, D.B., Cornell, M.E., Bender, R., 2009, ApJS, 182, 216

Krauss, L.M., 2006, Invited Review talk, Neutrino 2006, to appear in Proceedings [arxiv.org/abs/hep-ph/0702051]

Kroupa, P., 2001, MNRAS, 322, 231

Li B., Barrow J.D., Mota D. F. , 2007, Phys. Rev. D76, 104047

Lima Neto, G.B., Gerbal, D., Márquez, I., 1999, MNRAS, 309, 481

Linde A.D., 2008 , Lect. Notes Phys. 738, 1

Lubini, M., Tortora, C., Näf, J., Jetzer, Ph., Capozziello, S., 2011, Eur. Phys. J. C., 71, 1834

S. S. McGaugh, 2012, AJ, 143, 40

Mamon, G.A., Lokas, E.L., 2005A, MNRAS, 362, 95 2005A, MNRAS, 362, 95

Mamon, G.A., Lokas, E.L., 2005B, MNRAS, 363, 705

Mamon, G.A., Lokas, E.L., 2006, MNRAS, 370, 1581

Manera M. & Mota D., 2006, MNRAS371, 1373

Mathews, W.G., Brighenti, F., 2003, ARA&A, 41, 191

Méndez, R.H., Riffeser, A., Kudritzki, R.-P., Matthias, M., Freeman, K.C., Arnaboldi, M., Capaccioli, M., Gerhard, O.E., 2001, ApJ, 563, 135

Mota, D. F., Shaw, D. J. 2006, Phys.Rev.Lett., 97, 151102

Mota D. F., 2008, JCAP 09006

Mota, D.F., Salzano, V., Capozziello, S., 2011, Phys. Rev. D, 83, 084038 (Paper I)

Napolitano, N.R., Arnaboldi, M., Freeman, K.C., Capaccioli, M., 2001, A&A, 377, 784

Napolitano, N.R., Arnaboldi, M., Capaccioli, M., 2002, A&A, 383, 791

Napolitano, N.R., Romanowsky, A.J., Coccato, L., Capaccioli, M., Douglas, N.G., Noordermeer, E., Gerhard, O., Arnaboldi, M., De Lorenzi, F., Kuijken, K., Merrifield, M.R., O'Sullivan, E., Cortesi, A., Das, P., and Freeman, K.C., 2009, MNRAS, 393, 329

Napolitano, N.R., Romanowsky, A.J., Capaccioli, M., Douglas, N.G., Arnaboldi, M., Coccato, L., Gerhard, O., Kuijken, K., Merrifield, M.R., Bamford, S.P., Cortesi, A., Das, P., Freeman, K.C., 2011, MNRAS, 411, 2035 (N+11)

Napolitano, N.R., Capozziello, S., Romanowsky, A.J., Capaccioli, M., Tortora, C., 2012, ApJ, 748, 87

Navarro, J.F., Frenk, C.S., White, S.D.M., 1996, ApJ, 462, 563

Navarro, J.F., Hayashi, E., Power, C., Jenkins, A.R., Frenk, C.S., White, S.D.M., Springel, V., Stadel, J., Quinn, T.R., 2004, MNRAS, 349, 1039

Olive, K. A., Pospelov, M., 2008, Phys. Rev. D, 77, 043524

Oyaizu, H., et al., 2008, Phys. Rev. D, 78, 123524

Padmanabhan, T. 2003, Phys. Rep., 380, 235

Peacock, J.A., 2003, Cosmological Physics, Cambridge University Press, Cambrige, UK

Peebles, P.J.E., Rathra, B. 2003, Rev. Mod. Phys., 75, 559

Peng, E.W., Ford, H.C., Freeman, K.C., 2004, ApJ, 602, 685

Persic, M., Salucci, P., Stel, F., 1997, MNRAS, 281, 27

Postman, M., et al., 2012, Astrophys. J. Supp. 199, 25

Prugniel, P., Simien, F., 1994, A&A, 321, 111

Puzia, T.H., et al., 2004, A&A, 415, 123

Romanowsky, A.J., Douglas, N.G., Arnaboldi, M., Kuijken, K., Merrifield, M.R., Napolitano, N.R., Capaccioli, M., Freeman, K.C., 2003, Science, 301, 1696

Romanowsky, A.J., Strader, J., Spitler, L.R., Johnson, R., Brodie, J.P., Forbes, D.A., Ponman, T., 2009, AJ, 137, 4956

Sahni, V., Starobinski, A. 2000, Int. J. Mod. Phys. D, 9, 373

Salucci, P., Frigerio Martins, C., Lapi, A., arXiv:1102.1184

Sanchez, A.G. et al. 2006, MNRAS, 366, 189

Schneider, P., Ehlers, J., Falco, E.E., 1992, Gravitational Lenses (Gravitational Lenses, XIV, (New York: Springer-Verlag Berlin Heidelberg), also Astronomy and Astrophysics Library)

Schuberth, Y., Richtler, T., Hilker, M., Dirsch, B., Bassino, L.P., Romanowsky, A.J., Infante, L., 2010, A&A, 513, A52

Seljak, U. et al. 2005, Phys. Rev. D, 71, 103515

Shen, J., Gebhardt, K., 2010, ApJ, 711, 484

A. A. Starobinsky, 2007, JETP Lett. 86, 157-163

R. A. Swaters, R. H. Sanders, S. S. McGaugh, 2010, ApJ, 718, 380

Tegmark, M. et al. 2004, Phys. Rev. D, 69, 103501

Teodorescu, A.M., Méndez, R.H., Bernardi, F., Riffeser, A., Kudritzki, R.P., 2010, ApJ, 721, 369

Tonry, J.L., Dressler, A., Blakeslee, J.P., Ajhar, E.A., Fletcher, A.B., Luppino, G.A., Metzger, M.R., and Moore, C.B., 2001, ApJ, 546, 681

Vikhlinin, A., Markevitch, M., Murray, S.S., Jones, C., Forman, W., Van Speybroeck, 2005, ApJ, 628, 655

Woodley, K.A, Gómez, M., Harris, W.E., Geisler, D., Harris, G.L.H., 2010, AJ, 139, 1871

Zitrin, A., et al., 2011, ApJ, 742, 117

Zitrin, A., et al., 2012, MNRAS, 420, 1621

APPENDIX

TABLE 5

Spiral galaxies: Scalar field. Column 1: Name of the LSB galaxy. Column 2: Coupling constant of scalar field and star component. Column 3: Coupling constant of scalar field and gas component. Columns 4: Scalar field interaction length. Column 5: Stellar mass-to-light ratio in the V-band.

	β_{star}	β_{gas}	L (kpc)	Y_* ($Y_\odot$)
UGC1230	$4.831^{+3.910}_{-2.243}$	$1.167^{+0.159}_{-0.167}$	$57.778^{+94.884}_{-23.604}$	$0.201^{+0.474}_{-0.139}$
UGC1281	$0.283^{+2.620}_{-0.234}$	$1.347^{+0.090}_{-0.077}$	$7.687^{+13.748}_{-3.482}$	$2.775^{+0.493}_{-2.574}$
UGC3137	$4.400^{+4.032}_{-1.884}$	$1.970^{+0.021}_{-0.019}$	$484.99^{+2106.55}_{-382.01}$	$0.409^{+0.781}_{-0.294}$
UGC3371	$3.452^{+3.644}_{-1.985}$	$1.726^{+0.316}_{-0.178}$	$10.543^{+28.614}_{-6.046}$	$0.350^{+1.283}_{-0.268}$
UGC3851	$1.243^{+2.258}_{-0.476}$	$0.119^{+0.315}_{-0.086}$	$2.203^{+3.199}_{-0.933}$	$2.144^{+1.866}_{-1.806}$
UGC4173	$4.096^{+3.490}_{-2.389}$	$0.700^{+0.368}_{-0.528}$	$11.995^{+51.799}_{-7.377}$	$0.201^{+0.657}_{-0.138}$
UGC4278	$3.479^{+3.347}_{-1.573}$	$1.328^{+0.063}_{-0.062}$	$96.241^{+102.113}_{-33.083}$	$0.242^{+0.498}_{-0.176}$
UGC4325	$0.316^{+2.485}_{-0.268}$	$2.838^{+0.407}_{-0.291}$	$3.853^{+6.053}_{-1.901}$	$2.924^{+1.420}_{-2.716}$
UGC5721	$0.180^{+0.512}_{-0.132}$	$3.486^{+1.049}_{-0.459}$	$1.454^{+0.567}_{-0.586}$	$1.468^{+0.866}_{-1.116}$
UGC7524	$0.721^{+0.278}_{-0.222}$	$1.462^{+0.292}_{-0.547}$	$1.022^{+0.394}_{-0.156}$	$5.395^{+1.356}_{-1.537}$
UGC7603	$0.092^{+0.204}_{-0.066}$	$1.782^{+0.038}_{-0.037}$	$31.176^{+105.046}_{-19.245}$	$0.052^{+0.071}_{-0.035}$
UGC8286	$3.069^{+2.092}_{-0.923}$	$2.169^{+0.073}_{-0.054}$	$34.052^{+167.546}_{-25.431}$	$0.161^{+0.151}_{-0.101}$
UGC8837	$0.124^{+0.327}_{-0.092}$	$2.009^{+0.263}_{-0.189}$	$2.460^{+6.386}_{-0.121}$	$0.111^{+0.289}_{-0.082}$
UGC9211	$3.575^{+3.367}_{-1.883}$	$1.579^{+0.439}_{-0.192}$	$5.670^{+13.011}_{-2.933}$	$0.280^{+0.858}_{-0.204}$
UGC10310	$0.122^{+0.582}_{-0.091}$	$1.543^{+0.701}_{-0.278}$	$3.450^{+9.622}_{-2.397}$	$2.535^{+0.465}_{-1.234}$